MEMS Laser Scanners: A Review

Sven T. S. Holmström, Utku Baran, and Hakan Urey, *Senior Member, IEEE*

***Abstract*— Laser scanners have been an integral part of MEMS research for more than three decades. During the last decade, miniaturized projection displays and various medical-imaging applications became the main driver for progress in MEMS laser scanners. Portable and truly miniaturized projectors became possible with the availability of red, green, and blue diode lasers during the past few years. Inherent traits of the laser scanning technology, such as the very large color gamut, scalability to higher resolutions within the same footprint, and capability of producing an always-in-focus image render it a very viable competitor in mobile projection. Here, we review the requirements on MEMS laser scanners for the demanding display applications, performance levels of the best scanners in the published literature, and the advantages and disadvantages of electrostatic, electromagnetic, piezoelectric, and mechanically coupled actuation principles. Resonant high-frequency scanners, low-frequency linear scanners, and 2-D scanners are included in this review. [2013-0235]**

***Index Terms*— Laser displays, MEMS scanners, portable projectors.**

I. Introduction

SINCE the first scanning silicon mirror was published in 1980 [1] microelectromechanical systems (MEMS) for light scanning has seen a vast array of applications. Early MEMS scanners focused on imaging applications such as confocal microscopy [2]–[7], bar code reading [8], and finger print sensing [9]. Around the turn of the new millennium optical cross-connects (OXC) technology [10] was the primary driver for 2D scanners. It has now been supplanted in this role by the miniaturized projection display with its large demands on frequency, scanning angle, and footprint [11]. Other applications include optical coherence spectroscopy (OCT) [12], [13], and the retinal scanning display (RSD) [14], printing [15], head-up displays [16] as well as light detection and ranging (LIDAR) systems for the automotive industry [17], [18].

For imaging applications, demands on the laser scanner are not as high as in displays. The performance of scanned imaging systems are typically limited by (i) optics, which demand small focused spot and dynamic focusing and (ii) low signal levels that demand higher integration time and slow scanning speed. Therefore, majority of the highest performing scanners to be discussed in this paper are developed for displays, which will be the main focus of this paper.

Manuscript received July 29, 2013; revised December 3, 2013; accepted December 15, 2013. Date of publication January 16, 2014; date of current version March 31, 2014. S. Holmström and U. Baran contributed equally to this paper. Subject Editor O. Solgaard.

S. T. S. Holmström, and H. Urey are with the Department of Electrical Engineering, Koç University, Istanbul 34450, Turkey (e-mail: sholmstrom@ku.edu.tr; hurey@ku.edu.tr).

U. Baran is with the Department of Electrical Engineering, University of Washington, Seattle, WA 98467 USA (e-mail: ubaran@uw.edu).

Color versions of one or more of the figures in this paper are available online at http://ieeexplore.ieee.org.

Digital Object Identifier 10.1109/JMEMS.2013.2295470

A. MEMS in Displays

For display applications, there are three types of architectures where MEMS technology have been used: (1) *2-dimensional arrays* acting as spatial light modulators (SLM). The most mature technology is Texas Instrument's Digital light processor (DLP), using Digital micromirror devices (DMD) [19], [20], where the MEMS component is a large array of bistable micromirrors. These devices have a one-to-one relationship between the number of mirrors and pixel count. (2) *Scanned 1-dimensional arrays*, where a 1D array is scanned to generate the full 2D image. Two well-known implementations, both using diffractive-type optical components, are the grating light valve technology (GLV) [21] and the interferometric modulator technology (iMoD) [22]. These technologies are today owned by Silicon Light Machines and Qualcomm, respectively. (3) *2-dimensional laser scanning devices* - flying spot devices - on the other hand, where a single modulated laser source is scanned simultaneously in two dimensions [23], as detailed in this paper. A comprehensive account of the competing MEMS technologies can be found in [24].

B. Lasers in Displays

The first laser displays were proposed already in the 1960's, but the commercial viability of the technology, especially miniaturized implementations, was limited due to bulky and expensive laser sources [25]. Early examples of compact laser scanners appeared in the late 90s [26]–[29]. The first commercially available display system using MEMS-based laser scanning was the RSD, which creates a virtual image directly onto the eye of the user with laser raster scanning [14]. RSD systems have existed for over a decade, but more interest is now directed towards mobile projector displays [30]. However, the development of miniaturized projectors with full color was hampered by the bulky frequency doubling schemes that was typically used as the green laser component [31], [32]. In 2010 direct emission green diode lasers became available, enabling compact red-green-blue (RGB) display engines. This enabled portable and truly miniaturized laser projectors, the beginning of which we are seeing right now.

C. Pico-Projectors

The three currently competitive technologies for miniaturized projectors are MEMS laser scanning, DMD, and liquid crystal on silicon (LCoS) displays [33]. DLP and LCoS are both examples of SLMs. LCoS is similar to DLP in regards to working principle, but the reflected light is modulated by

1057-7157 © 2014 IEEE. Personal use is permitted, but republication/redistribution requires IEEE permission.
See http://www.ieee.org/publications_standards/publications/rights/index.html for more information.

liquid crystals instead of bistable mirrors. The main advantages of laser scanning are the high color gamut, scalability of resolution within the same footprint, and an always-in-focus image [31], [34]. The two latter are especially important for miniaturized displays. Compared to SLM-based systems the direct modulation of the lasers for each pixel leads to a shift of architectural complexity from optomechanics to electronics. The direct modulation also facilitates good power efficiency and inherently high contrast [35]. The major drawback of the laser scanning approach is laser speckle.

D. Laser Scanners

Traditional techniques for laser scanning include acousto-optic scanners, polygon scanners, and galvanometric scanners. MEMS scanners are desired since they allow miniaturization, low power consumption, as well as much superior performance at resonant high frequency actuation. A useful and inclusive classification of MEMS scanners was formulated in [23]. With a slightly simplified version of this optical MEMS scanners can be classified according to the following three categories: (1) *operation principle* (reflective mirror, refractive lens, and diffractive grating), (2) *actuation* principle (mainly electrostatic, electromagnetic, piezoelectric, and electrothermal), and (3) *fabrication technology* (e.g. bulk micromachining, surface micromachining, and hybrid fabrication methodologies). However, the vast majority of high performing display scanners are torsional mirrors made by silicon bulk micromachining with only actuation method varying.

In this paper the current state of MEMS laser scanners are reviewed and discussed. The main focus is on applicability for miniaturized projectors and wearable displays. It is the first review of its kind, but a few earlier reviews have partly treated the same topic [11], [36], [37]. Included are comprehensive comparisons of published scanners and evaluations of the future challenges of each technology. Display applications have the highest physical demands on the scanner and as the primary driver of development it is particularly useful to focus on the specific requirements different screen resolution translate to. It is the authors' hope that the information provided can be of service to everyone planning to design or simply choose a laser scanner for display as well as various imaging applications. The aim is to be as inclusive as possible regarding operation principles, but to focus on the scanner architectures that have produced the highest performing scanners.

In Section II scanner requirements and performance metrics are introduced and discussed. In Section III the commonly utilized actuation principles are compared. In Sections IV, V, and VI published fast scanners, slow scanners, and 2D scanners, respectively, are discussed and compared. Finally, in section VII the paper is concluded with a discussion on economies of scale, commercialization, and a roadmap for imaging of MEMS scanners.

II. Requirements for MEMS Laser Scanner Displays

To gauge the performance of a display scanner one needs to consider working frequency, scan angle, mirror size, mirror flatness (dynamic and static), good mode separation (resonant scanners), and linearity (non-resonant scanners) [26]. The two latter points are relevant to image quality, while the others directly determine limits for resolution and image size. A resonant scanner design needs to strike a balance where the combination of scan angle, resonance frequency, and mirror size is enough for the desired resolution, while still keeping the mirror optically flat to avoid image distortions. For non-resonant slow scanners linearity is often the most difficult problem to solve.

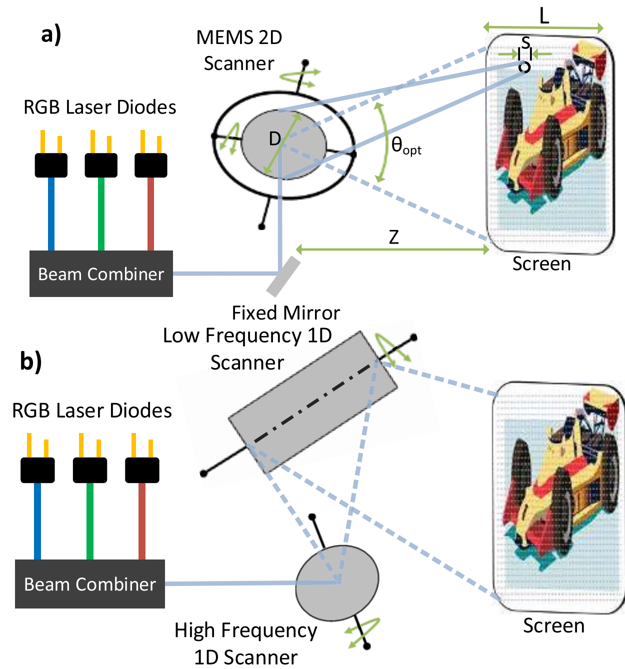

Fig. 1. Schematic of a flying spot laser projector. (a) 2D scanning mirror architecture. (b) Two-scanning-mirror architecture where each mirror is responsible for one axis.

The laser spot projector can be implemented either with a single dual-axis mirror or with two separate, orthogonal single-axis scanners, as shown in Fig. 1 [38], [39]. One important difficulty with dual-axis scanners is the crosstalk between the two axes. With increasing display resolution it becomes harder to keep the crosstalk to acceptable levels, which would be the main reason to choose the bulkier two-mirror architecture. To create the proper color mix for each pixel, all three lasers have to be modulated simultaneously.

A. Resolution

An in-depth account of scanner requirements is given in [26], on which much of the following is based. The most common system architecture is raster scanning, where a low frequency, linear vertical scan (quasistatic) is paired with an orthogonal high frequency, resonant horizontal scan. An alternative to this is the bi-resonant Lissajous scanner, which is described further in the introduction of Section V. For the raster scanner the vertical scan is often assumed to be 60 Hz (video frame rate). The two main contributors to the number of resolvable spots are the scan angle, θ, and the clear mirror aperture, D. In the literature three different definitions are commonly used for the scan angle: the zero-to-peak

mechanical, θ_{mech}, peak-to-peak mechanical, $\theta_{p-p\,mech}$, and full optical, θ_{opt}. For a torsion mirror scanner $\theta_{opt} = 2\theta_{p-p\,mech} = 4\theta_{mech}$. In this paper θ_{opt} is used if not otherwise specified. Assuming a small angle (paraxial approximation) the number of resolvable spots along the horizontal direction (N_h) can be written as

$$N_h = \frac{L}{s} = \frac{4\theta_{mech} z}{a\lambda \frac{z}{D}} = \frac{\theta_{opt} D}{a\lambda} \quad (1)$$

where, additionally, L is the screen length, s the spot size, z the distance to the screen λ the longest system wavelength, and a (typically between 0.75 and 2) a shape factor determined by the definition of spot size (amount of overlap between adjacent spots), mirror shape, angle of incidence, fraction of the scanline used for writing, and beam profile [26], [40]. See the sketch in Fig. 1(a). From (1) it is understood that the $\theta_{opt} \cdot D$-product determines the number of resolvable spots along the axis. The number of resolvable spots along the vertical axis, N_v, can be calculated from the refresh rate of the display (F_r), the horizontal frequency (f_h), the fraction of the time used for retrace of the vertical scanner moving at constant speed (K_{rt}), and the K_{ub} constant which is 1 for unidirectional writing and 2 for bidirectional writing [26].

$$N_v = \frac{f_h K_{ub} K_{rt}}{F_r} \quad (2)$$

That is, the ratio of horizontal scan frequency to display refresh rate determines the number of vertical lines possible. In the bidirectional writing scheme ($K_{ub} = 2$) the scanner writes two lines during one scan cycle, and hence increases the light source utilization by a factor of 2 and reduces the required horizontal scanner frequency by half. Although unidirectional writing schemes can provide better line to line positional uniformity, bidirectional schemes are more common and are used for all calculations in this paper [30]. It is also possible to further reduce the frequency burden by using multiple beams with a single mirror. This has been demonstrated [41], but there are very few implementations and is not considered further in this text. Given a fixed refresh rate (vertical scanning frequency) each resolution can be translated into fast scanner requirements expressed as limits of $\theta_{opt} \cdot D$ -product and f_h. The limit for $\theta_{opt} \cdot D$ is set by the horizontal pixel count, while f_h is limited by the vertical pixel count. In reverse, they are used as metrics to compare fast scanners. To further facilitate easy comparison of fast scanners operating at different frequencies the $\theta_{opt} \cdot D \cdot f_h$-product is used as a single metric indicating the pixel rate made possible by a specific fast scanner. For requirements on pixel timing we refer to [26]. Additional discussion on requirements for linear scanners can be found in Section V.

B. Dynamic Deformation

For evaluation of a scanner design it is important to understand how different features interact with each other. Tradeoffs between scan angle and mirror width with respect to resolution are developed in detail in [14]. For a fixed $\theta_{opt} \cdot D$ an increasing D leads to larger mirror deformation, lower maximum frequency, and increasing cost and footprint.

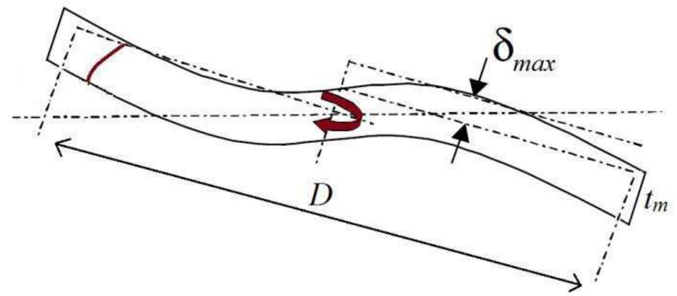

Fig. 2. Sketch of the dynamic mirror deformation.

On the other hand it will provide less tight optomechanical tolerances and lower flexure stress. For high performance, resonant scanners, the mirror deformation tends to be the most difficult part to solve. High acceleration forces, caused by the mechanical deflection, result in mirror bending, which in turn leads to optical distortion of the image (Fig. 2). Dynamic deformation of the mirror, defined as the deviation from linearity, can be predicted using Brosens's formula below, which uses the unevenly distributed forces due to acceleration across the mirror surface,

$$\delta_{max} = 0.217 \frac{\rho f^2 D^5 \theta_{mech}}{E t_m^2} \quad (3)$$

where, ρ is the material density, E the modulus of elasticity, f the scanner frequency and t_m the mirror thickness [6], [42].

To keep the spot diffraction limited, the maximum mechanical mirror deformation (δ_{max}) should not exceed $\lambda/10$ of the shortest system wavelength [26]. Note that δ_{max} is proportional to D^5. Hence, if the system performance is deformation limited, significant gains can be attained by slightly reducing the mirror size. These constraints are the main reason to why surface micromachining is generally not used for high performance scanners. In addition to the thicker substrate bulk micromachining allows for, mirror reinforcement structures and additional mechanical connections to the mirror frame can also substantially reduce the dynamic deformation. The earliest studies on well-characterized MEMS mirrors were published in 2000 by Urey et al. [26] and Conant et al. [43]. Common methods to measure dynamic deformation are monochromatic stroboscopic interferometry and stroboscopic white light interferometry [26], [44]. Table I shows $f_h, \theta_{opt} \cdot D$, and maximum pixel clock frequency requirements for a fast scanner needed to address various image resolutions. Bidirectional raster scanning and 60 Hz refresh rate is assumed. The values are calculated based on the equations found in [26]. Exact values will always depend on the specific implementation, but the ones used here are typical and internally consistent.

III. Actuation Principles

High performance laser display applications require large displacements of a large aperture mirror coupled with high motion precision. Resonant scanners make use of high mechanical quality factor (Q) to reach the required angle. At atmospheric pressure a very high drive torque is required to overcome the air damping. This problem can be solved by use

TABLE I
$\theta \cdot$ D AND HORIZONTAL FREQUENCY REQUIREMENTS OF VARIOUS RESOLUTIONS FOR DISPLAYS USING BIDIRECTIONAL RASTER SCANNING ARCHITECTURE

	VGA	WVGA	SVGA	HD720	HD1080
Horizontal Pixels	640	854	800	1280	1920
Vertical Pixels	480	480	600	720	1080
$\theta_{opt} \cdot D$ - Req. [deg·mm]	28.1	37.5	35.2	56.3	84.4
f_h - Req. [kHz]	18	18	22.5	27	40.5
Max. Pixel Clock Freq. [MHz]	38.5	51.4	60.2	115.5	259.9

TABLE II
COMPARISON OF PROPERTIES OF ACTUATION PRINCIPLES

Category	Electrostatic	Electromagnetic	Piezoelectric
Preferred Type	Comb drive	Moving coil	PZT film
Simple Fabrication	✓✓✓	✓✓✓	✓✓
Large Displacement	✓✓	✓✓✓	✓
High Force	✓	✓✓	✓✓✓
Low Power	✓✓	✓	✓✓✓
Low Voltage	✓	✓✓✓	✓✓
Compactness	✓✓✓	✓	✓✓✓
Linearity	✓	✓✓✓	✓✓

of a vacuum package, which is costly and leads to a different set of technical problems [45]. In addition, the suspended mass becomes heavy due to large mirror size and dynamic flatness requirements [46]. The non-resonant operation of the vertical scan also demands a high torque to overcome the flexure stiffness that cannot be set very low due to requirements for shock and handling robustness.

The three main actuation principles to be considered here are electrostatic actuation (ES), electromagnetic actuation (EM), and piezoelectric actuation (PE). Much research has also been carried out on electrothermal (ET) scanners [47]–[50]. Due to the inherently long response times of ET devices, scanners based on this technology is not very suitable for display applications, but could possibly be used to actuate a slow scanner used in combination with a fast scanner using a different actuation principle.

When comparing scanners for commercial use, the most critical aspects to consider are: enabled resolution, fabrication simplicity, power efficiency, voltage requirement, robustness, compactness, and long-term stability. Each actuation principle has advantages in some aspects while having disadvantages in others. Table II compares qualitatively the properties of each actuation principle qualitatively based on the highest performing scanners designed for miniaturized displays.

A. Electrostatic Actuation

ES actuation was the first actuation method used for MEMS scanners and comprises the vast majority of the published literature. The two main reasons for this are: fabrication compatibility with any facility with MEMS capability without the need of any unusual material and ease of integration into the full system. In contrast, PE actuators require the deposition of a piezoelectric material while the moving coil EM actuators require a magnet to be included in the final package.

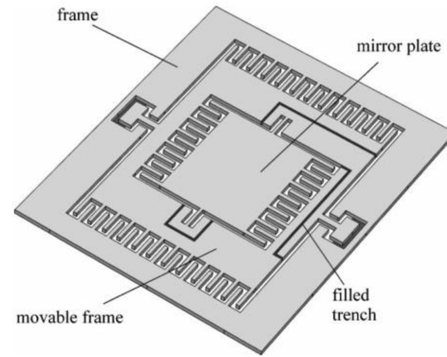

Fig. 3. Layout of a ES 2D scanner. The filled trenches are needed for electric isolation. Reprinted with permission from [51].

The working principle of ES actuation relies on the attraction of two oppositely charged plates. The electrostatic force between two plates can be expressed as

$$F_{es} = \frac{A\varepsilon V^2}{2g^2}, \tag{4}$$

where A is the overlap area of the plates, ε is the dielectric constant of the medium (i.e. air), V is the voltage difference applied between the plates, and g is the gap between the plates. There are two main schemes of electrostatic actuation: comb actuation and parallel-plate actuation. Much of the early work made use of parallel plate actuation, indeed the first silicon scanning mirror published by Petersen in 1980 was of this type [1], [52]. Parallel-plate actuation has great utility for many applications with a low $\theta \cdot$D-requirement and is still favoured for bi-stable mirrors, as in DLP [19]. The basic version of the parallel plate actuator is practically very limited in scan range, since very high actuation voltages are soon required due to large electrode separation. On the other hand, comb drive actuation has been the preferred actuation method for ES high frequency scanners since the turn of the century. In this scheme multiple plates are attached to each other like comb fingers to constitute two interdigitated rows, one static and one free to move, as illustrated in Fig. 3 [53]. This configuration allows for larger motion and the imparted force to be much more evenly distributed over the motion. The first comb finger driven micro actuator was described by Tang et al. in 1990, while the first vertical (out-of-plane) comb actuator was made by Selvakumar et al. in 1995 [54], [55].

ES actuation provides long-term stability, size advantages, and fabrication schemes which are easier to render CMOS compatible. On the other hand, it requires high voltages to operate, and is sensitive to inexactness in microfabrication due to the pull-in phenomenon. Particularly comb actuation is prone to fail over large travel ranges due to the interaction of a nonlinear electrostatic force with a linear elastic restoring force [56]. The pull-in problem is treated in detail in [57] and [58]. This nonlinear leads to a time-varying torsional stiffness, either named as spring stiffening or spring softening,

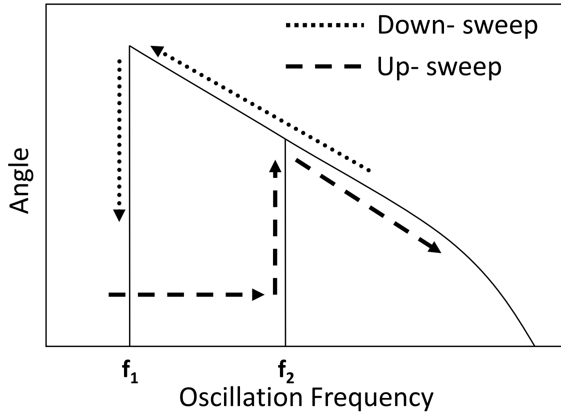

Fig. 4. Sketch of a typical frequency response of parametric ES scanner. The actuation frequency is typically double the oscillation frequency.

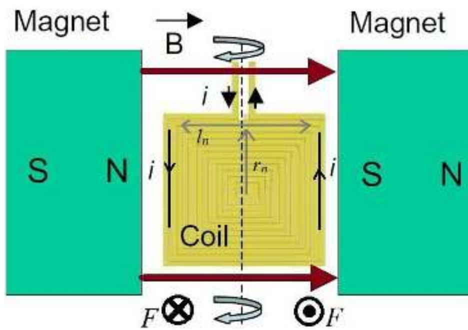

Fig. 5. General configuration of a torsional scanner with coils and magnets for a moving coil actuation [61]. To enhance the Lorentz force, more than 2 magnets can be used by engineering the positions of the magnets [62]. Reprinted with permission from [61].

depending on how the resonance frequency changes with increasing deflection. The sketch in Fig. 4 shows the typical frequency response of a parametric scanner exhibiting ES spring softening. Parametric oscillators can be actuated at $2f/n$, where n is a positive integer and f the natural frequency. The deflection is higher for low n. Subsequently, ES scanners are typically actuated at 2f. This is described further in [59] and [60].

B. Electromagnetic Actuation

There are two major EM schemes in use: moving magnet and moving coil. The former uses an external coil together with either a bulk magnet or a thin magnetic film deposited onto the device. It offers simple microfabrication and eliminates the need of electrical contacts since the actuation is driven with an off-chip coil. In the moving coil scheme, a coil is fabricated onto a scanner and external magnets are used to provide a static magnetic field, as illustrated in Fig. 5 [61], [62]. The configuration makes use of the Lorentz force acting on the coil when a current is present. Lorentz force, magnetic torque, and the power consumption of the coil can be calculated as below

$$F_{Lorentz} = Bil, \quad (5)$$

$$T_{mag} = 2\sum_{n=1}^{N} Bil_l r_n, \quad (6)$$

$$P_{coil} = i_{rms}^2 R_{coil}, \quad (7)$$

where B is the magnetic field, i the current, l the length of the conductor, N the number of coil turns, r_n the distance of the nth coil turn from the center, and R the resistance of the coil.

Since the actuation force naturally scales with the area, comparative efficiency of EM versus ES actuation increases with increasing mirror size [11]. EM actuation also has a more linear response than the competing principles, rendering it the most suitable for linear slow scanners. However, there are also drawbacks. The achievable performance of the electromagnetically actuated MEMS scanner is limited by the large thermal dissipation of the coil. High conducting currents inside a coil also consume significant power, which is a particularly critical aspect for mobile devices. Additionally, magnets strong enough for high performance take up a significant space and might require magnetic shielding. This leads to total package sizes that are larger than the ones for comparable ES and PE scanners.

C. Piezoelectric Actuation

Thin film PE actuation has had somewhat of a late arrival to MEMS laser scanning due to lack of convenient fabrication techniques and machinery, although it provides several advantages over other methods [63]. As reliable and convenient fabrication techniques were developed for film deposition of piezoelectric materials it has become accepted as a major actuation principle for MEMS scanners during the last decade. An alternative to thin filmis the use of stack or bulk piezoelectric actuators. They are typically bulky and require hybrid fabrication, which leads to a less streamlined process [15], [64]. On the other hand, they are readily available, low-cost, and can offer high force.

The first attempts to fabricate piezoelectric actuated MEMS used thin film materials such as ZnO and AIN. Lead zirconate titanate (PZT) is in comparison more cumbersome to deposit, but a film of equal thickness will typically develops ten times larger force [65]. Hence, PZT is now the most popular material for MEMS scanner actuation. Recently, Hishinuma et al. demonstrated a sputtered PZT film with a piezoelectric coefficient ~70% higher than in previously reported sputtered PZT films [66].

The working principle of PZT thin film based actuators for MEMS scanners relies on the stress emanating from the expansion of the PZT film in x direction when voltage is applied in the z direction (Fig. 6). Relevant piezoelectric coefficients for this effect are e_{31} and d_{31}, which translate the strain and the stress, respectively, in x direction as a function of E field in z direction [65]. The corresponding coefficients can be measured directly by the methods presented in [67].

PE actuation has several distinct advantages. In contrast to EM scanners no magnets or shielding is required, while PE devices simultaneously operate at a much lower voltage than typically needed for ES scanners. PE films have a large energy density and deliver high forces, but a major drawback is the short stroke length [63], [69]. To reach the relatively large scan angles needed for display scanners some sort of leverage is needed.

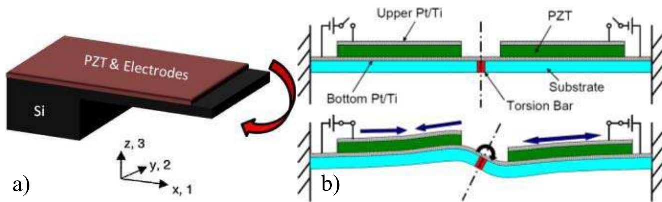

Fig. 6. Schematics to demonstrate the working principle of PZT actuators. (a) Bending of a unimorph Si cantilever due to stress induced by PZT layer. (b) One common technique in resonant PE torsion mirrors is the use of two unimorph cantilevers to impart torque on the torsion bar as shown in [68]. Reprinted with permission from [68].

The design limitations that govern PE scanners are rather different than those for EM and ES scanners. It is the opinion of the authors that there is still much room to further optimize scanner design to take full advantage of film-based PE actuation. High frequency PE scanners offer equal performance at much lower voltage levels than ES scanners and has a higher energy efficiency and much smaller package size compared to EM scanners [63], [69]. Moreover, PE actuators can measure deflection from the piezoelectric voltage of the separated electrode or the piezoelectric current charge [70], [71]. Thus, they can be used as angle sensors for closed-loop control of microscanners without any additional process or material.

D. Direct Drive Vs. Indirect Drive

In a scanner with direct drive the torque is imparted directly from the actuation mechanism to the frame containing the mirror. The indirect drive makes use of a favorable resonance mode to amplify a small motion in a larger mass to a considerably larger motion in the smaller mirror [38]. The usefulness of the principle of mechanical coupling has been demonstrated with EM [30], [38], [72], ES [13], [73]–[76], as well as PE actuation [44], [69]. In a mechanically coupled scanner there will be two possible scanning modes. In the in-phase mode the mirror and the larger mass will move together, while in the out-of-phase mode they will rotate in opposite directions. The angular coupling factor is the rotation ratio of the two masses. Typical frequency and phase responses of such a system designed to be used in the out-of-phase mode are shown in Fig. 7. The mechanical gain G is the angular coupling factor attained at ω_{op}, which is the desired operation frequency. Note that the angular coupling factor is maximum and equal to Q-factor at the dip frequency when the phase transition from in-phase to outer-phase. At the dip frequency, the outer frame deflection is at the noise level and all the energy is coupled to the inner frame. However, the overall scan angle is low at that frequency. Both G and Q are very important parameters to take into account in the design.

The direct drive is easier to design and has a richer literature, but for each of the major actuation principles there are distinct advantages. ES scanners using a direct drive are performance limited by damping power losses and the small actuator capacitance due to limited available area when the fingers are to be directly connected to the mirror [43], [77]–[82]. Experimental evidence for significant reductions in air damping of ES when the comb finger gaps are increased

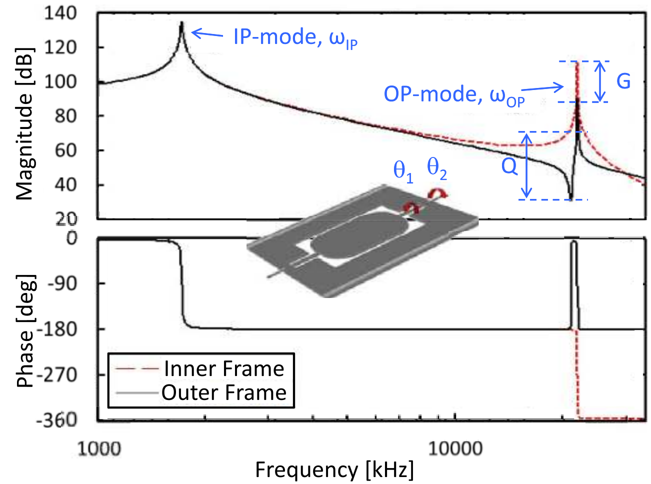

Fig. 7. Typical frequency and phase response for a scanner utilizing indirect drive and designed to operate at the out-of-phase mode (OP-mode) [73]. For this particular device the two frames move together in-phase (IP-mode). The gain (G) due to mechanical coupling is engineered to be large (often 5 to 20).

is shown in [83]. By removing the fingers completely from the high velocity inner frame and transferring them to a lower velocity outer frame, damping is significantly reduced, while at the same time not limiting the comb fingers to the perimeter of the mirror allows for higher actuation capacitance.

For EM scanners the best utility of mechanical coupling has been found in 2D scanners [30], [38]. In a gimbaled 2D scanner with a coil on the heavier outer frame a linear slow scan and a resonant fast axis can be driven simultaneously through signal superposition. This requires a high coupling factor to not disturb the linearity of the linear scan.

Due to the limited stroke of the actuator, PE scanners have the most to gain the most from mechanical coupling. The outer frame also makes it possible to apply force directly in the moving structure. Ideally the PE electrode should be designed to conform to the mode shape of the mechanical structure [84].

IV. Resonant Scanners (Fast Axis)

The highest performing resonant scanners are compared in Fig. 8. References and details of the individual scanners can be found in Table III [38]–[40], [44], [45], [52], [73]–[75], [77]–[80], and [85]–[96]. Only scanners with a working frequency above 15 kHz and a $\theta_{opt} \cdot D \cdot f_h$ higher than 500 deg $\cdot$ mm $\cdot$ kHz are included. No restriction was made due to measured or estimated dynamic deformation, but where data on dynamic deformation exist it is noted. Several of the listed scanners are additionally 2D-capable and as such described in Section VI.

Key insights can be drawn from Fig. 8 and Table III. ES actuated scanners constitutes a large portion of the published scanners, which is a reflection of the early adoption of them in this field. However, the voltage requirement of ES scanners is typically an order of magnitude larger than the other type of scanners. EM actuated scanners can reach high scan angles with a reasonable voltage requirement. Due to their superior performance in non-resonant scanning (see Section V), they have a clear advantage for realization of up to 720p resolution portable projector displays. On the other hand, PE actuation

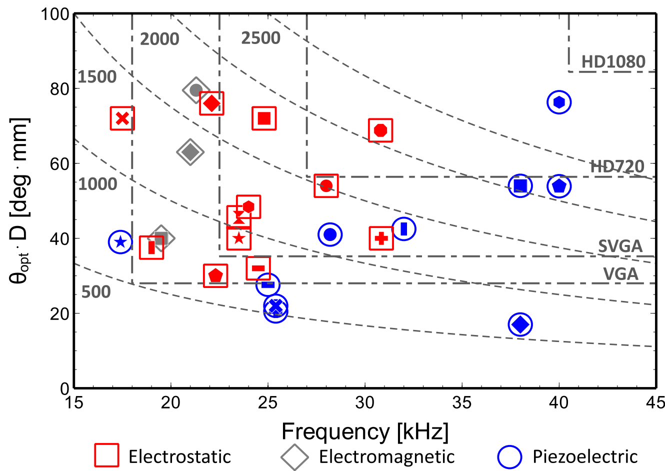

Fig. 8. Comparison of the highest performing resonant scanners in the literature working over 15 kHz. The requirements for f and $\theta_{opt} \cdot D$ assume 60 Hz refresh rate and bidirectional scanning. The dotted lines indicate $f_h, \theta_{opt} \cdot D$-levels to give a better understand for how this metric relates to resolution requirements. See Table III for information on the individual scanners.

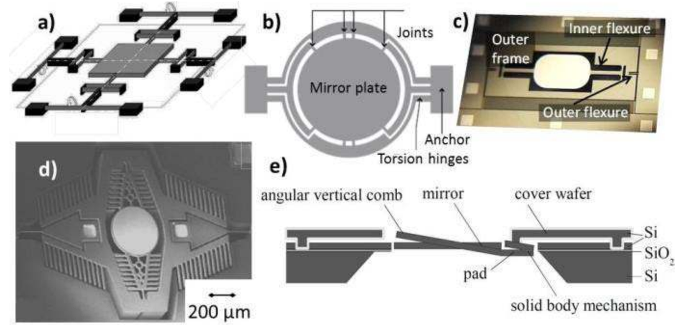

Fig. 9. Selection of ES scanners. (a) Gimbal-less silicon mirror with three degrees of freedom (tip-tilt-piston) [97]. Discussed in Section V. Reprinted with permission from [97]. (b) In this design by Hsu et al. the dynamic deformation is kept to a minimum by a butterfly shaped reinforcement (not shown) and a complicated suspension structure [87]. Reprinted with permission from [87]. (c) This scanner by Arslan et al. consists of a mechanically coupled system with two cascaded platforms [73]. The mechanical coupling is utilized to reach high deflection with relatively small comb finger motion. (d) SEM of a fabricated 2D microscanner [81]. Reprinted with permission from [81]. (e) Schematic illustration of the scanners presented by Jung et al. [94]. During wafer bonding stamps on the cover wafer are pressing on the deflection pads of the mirror wafer. Through these so called solid body mechanisms the force is coupled via coupled hinges into vertical deflection of the comb drive counter electrode. Reprinted with permission from [94].

is by a large margin the highest performing technology for >30 kHz resonance frequency devices, whereas EM and ES actuations fall short to provide competitive scanners in this regime. It is reasonable to see indirectly driven PE actuated scanner as a main candidate for at the least the fast axis in the next generation high resolution (1080p) displays where ~40 kHz resonance frequency is required.

A. Electrostatically Actuated Scanners

There has been an intense research on ES MEMS scanners for more than one decade [73], [74], [77], [79], [85], [98]. The first well-characterized high-frequency ES scanner for display applications was published in 2000 by Conant et al. [43]. It features a 0.55 mm circular mirror resonating at 34 kHz driven in a direct-drive configuration with staggered vertical combs (SVC, See Section V-A for more discussion of SVC devices.). Scanners up to 42 kHz were designed and built with the same technology, well beyond what had existed up to that point. Importantly the mirror was dynamically measured and was found to be optically flat. Cho et al. from Samsung Electronics Co. presented a scanner that has a long SVC actuator attached directly to the mirror [77]. Researchers from the same company published in 2006 a fast scanner with an unusual two level SVC actuation [79]. The drive consists of combs at three different levels, with static comb drives above as well as below the moving combs. This type of geometry is otherwise mainly used for quasistatic scanning. Researchers from Fraunhofer Institute for Photonic Microsystems (FhG-IPMS) presented a comb actuated mirror that meets the strict optical flatness requirement of $\lambda/10$ while producing optical angle of 40° at the resonance frequency of 30.84 kHz [Fig. 9(b)] [87]. Two major measures are made to reduce dynamic deformation. First, the 1 mm mirror plate is attached to a middle frame through 8 joints, which in turn is connected to the substrate with 6 parallel torsion springs. Second, a butterfly shaped reinforcement structure shaped from the handle silicon is left behind the mirror to increase its stiffness.

In the imaging field much effort has been directed towards MEMS scanners for miniaturized confocal microscopy, often for endoscopy applications. The starting point was [2] by Dickensheets and Kino, where two parallel-plate scanners are used in a monochromatic scanning confocal microscope. A much more recent MEMS-based confocal microscopy is described in [3]. There a single 2D raster scanner carries two separated, mechanically conjoined mirrors. One mirror is used for illumination, the other for output collection. To lower the power and avoid the high voltages required for raster scanning, unstable Lissajous scanning was implemented for this purpose in [4]. A frame rate of 2 Hz was accomplished.

As discussed in detail in Section III-D the indirect drive utilizing mechanical coupling has proven to be very useful for ES scanners, since it can decrease damping power losses as well as it allows for large actuator capacitance. Kurth et al. developed a parallel-plate scanner using indirect drive and showed an angular coupling ratio as high as 53 [75]. Yoda et al. presented in 2005 the first solution for a comb actuated scanner [74]. An implementation with higher performance was published by Arslan et al. [73]. In this 21.8 kHz device the mechanically coupled comb drive system consists of two cascaded platforms, the mirror and the comb bearing outer frame [Fig. 9(c)].

B. Electromagnetically Actuated Scanners

Significantly less work has been published on EM resonant scanner compared to ES devices, but it has been clearly shown that both techniques are competitive and that the chosen actuation principle will depend on the application. For very small form factors ES scanners have an advantage. As in the

TABLE III
DATA FOR HIGH FREQUENCY SCANNERS FOR THE COMPARISON IN FIG. 8

Actuation	Symbol in Fig. 7	Res. Freq. [kHz]	θ_{opt} [deg]	D [mm]	$\theta_{opt}\cdot D$ [deg·mm]	θopt·D·f [deg·mm·kHz]	Voltage [V]	Mechanical Design	Pressure	Notes and Reference
ES, Comb drive		28	36	1.5	**54**	**1512**	196	Indirect Drive, 1D	Reduced pressure	Model predicts deformation to be below λ/10. [85]
ES, Comb drive		22.1	76.0	1.0	**76**	**1679.6**	196	Indirect Drive, 1D	Atm.	Model predicts max. deformation to be above λ/10. [73]
ES, SVC Comb drive		24.8	48.0	1.5	**72**	**1782**	280	Direct Drive, SVC 1D	Atm.	FE analysis suggests 45 nm deformation at full deflection. [77]
ES, Steel Substrate, Parallel Plate		17.5			**72**	**1260**		Direct Drive, 2D	Atm.	The slow axis is a quasistatic EM drive. [40]
ES, Comb drive		30.8	40.0	1.0	**40**	**1216**		Direct Drive, 1D	Atm.	Deformation <27 nm RMS. [87]
ES, Comb drive		23.5	40.0	1.0	**40**	**940**		Direct Drive, 1D	Atm.	[78]
ES, SVC Comb drive		24.5	32.0	1.0	**32**	**784**	150	Direct Drive, 1D	Atm.	[79]
ES, Parallel Plates		19.0	26.8	1.4	**37.52**	**712.88**		Direct Drive, 2D	Reduced pressure.	Slow axis is a resonant EM drive. [52]
ES, AVC		22.3	30.0	1.0	**30**	**669**	140	Indirect Drive, 1D	Atm.	[74]
ES, Parallel Plates		24.0	22.0	2.2	**48.4**	**1161.6**	380	Indirect Drive, 1D	Atm.	Deformation <30 nm (280 μm thick device layer). [75]
ES, Comb drive		30.8	40	0.8	**68.8**	**1234**		Direct Drive, 2D	0.1 Pa.	Biresonant. Deformation < λ/10-limit according to the FE model. [45]
ES, Comb drive		23.5	38	1.2	**45.6**	**1071.6**	140	Direct Drive, 2D	Atm.	12.75 nm RMS at 7.5°. Quasistatic slow axis. [94]
EM, Moving Coil		21.3	53.0	1.5	**79.5**	**1693.35**		Indirect Drive, 2D	Atm.	Quasistatic slow axis. [38]
EM, Moving Coil		21.0	42.0	1.5	**63**	**1323**		Direct Drive, 1D	Atm.	[86]
EM, Moving Coil		19.5	40	1	**40**	**780**	4	Direct Drive, 1D	Atm.	[39]
PE, PZT Film		28.2	41.0	1.0	**41**	**1157.84**	60	Direct Drive, 1D	Atm.	Dyn. def. of 105 nm. Uses aerosol PZT on steel substrate. [88]
PE, PZT Film		38	17	1	**17**	**646**	6	Direct Drive, 1D	Atm.	[90]
PE, Bulk PZT		38	54	1	**54**	**2052**	5	Direct Drive, 1D	Atm.	[89]
PE, PZT Film		25.40	22.00	1.00	**22**	**558.8**	20	Direct Drive, 1D	Atm.	Titanium substrate. [91]
PE, PZT Film		25.4	41.0	0.5	**20.5**	**520.7**	42	Direct Drive, 1D	Atm.	Deformation below λ/10-according to FE model. [92]
PE, PZT Film		17.4	30	1.3	**39**	**678.6**	6	Direct Drive, 1D	Atm.	[96]
PE, PZT Film		25	27.6	1	**27.6**	**690**	10	Indirect Drive, 2D	Atm.	Biresonant scanning. [93]
PE, PZT Film		32	42.5	1	**42.5**	**1360**	7	Indirect Drive, 1D	Atm.	[95]
PE, PZT Film		40	38.5	1.4	**53.9**	**2156**	24	Indirect Drive, 1D	Atm.	Optical deformation up to 130 nm at ±4° mechanical angle. [44]
PE, PZT Film		40	54.5	1.4	**76.3**	**3052**	25	Indirect Drive, 1D	Atm.	[84]

case of ES scanners, but for slightly different reasons, indirect drive has proven to be a very important principle, especially for two axis scanners [38]. A majority of the reported high performance resonant EM MEMS scanners offer 2D scan, which are covered in Section VI-B.

Miyajima et al. presented a large 5 × 3.7 mm^2 mirror with a rotation of 16.8° optical scan angle in resonance at 2.7 kHz [99]. It requires around 350 mA current with Lorentz force excitation. Raboud et al. reported one of the few 1D electromagnetically actuated resonant MEMS laser scanners for microdisplays in the current literature [39]. The 19.5 kHz scanner is planned to be used alongside an EM slow scanner in a VGA capable projection system.

Reyne developed a 20 kHz resonance using moving magnet actuation with a 2 × 4 mm^2 mirror that can scan up to 5 deg [100]. Yalcinkaya et al. published a moving magnet 2D scanner with an electroplated soft magnetic NiFe layer actuated with an external coil [76]. Actuated at resonance the slow and fast axes create optical scan angles of 88° and 1.8°, respectively. Gokdel et al. presented a 1D soft magnetic steel scanner, where the bulk material also is the actuation material [101]. In [102] Weber et al. describe a process where nickel is electroplated onto a sacrificial layer, leading to a rotating mirror of pure nickel. It is presented as a cheap and simple alternative. Huang et al. presented a 2D moving magnet scanner using hard magnetic, electroplated CoNiMnP-film. The magnetic material is deposited in stripes to make use of the shape anisotropy to increase the efficiency [103]. Another example of the use of hard magnets is described in [104]. Here the magnets consist of neodymium powder kept in a polymer matrix. A disc of this material is attached directly to the reverse side of the mirror.

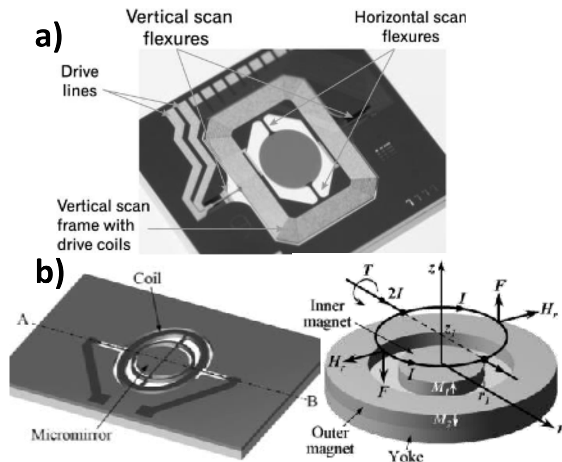

Fig. 10. Selection of EM scanners. (a) Bi-axial EM drive where the outer frame drives both axes through signal superposition [38], [46]. Reprinted with permission from [38]. (b) To the left a schematic view of the 2D EM micromirror presented in [72]. To the right schematics of the coil and concentric magnet assembly (M: magnetization, F: force, T: torque, H: magnetic field intensity, I: current). Reprinted with permission from [72].

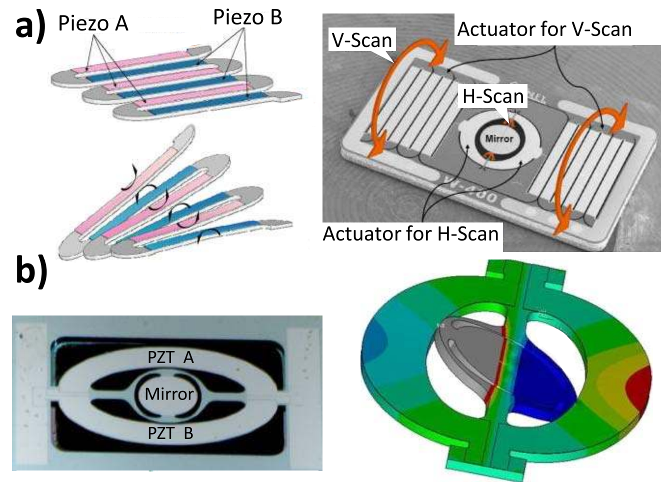

Fig. 11. Selection of PZT-based PE scanners. (a) The meander-beam solution, here shown to the left, by Tani et al. is the most successful solution for non-resonant PZT scanners so far . The angular displacement is accumulated along the turns of the springs. To the right is a 2D scanner combining this method with the PE resonant mechanism described in Fig. 6 [68]. Reprinted with permission from [68]. (b) PZT-driven 40 kHz scanner using mode coupling and a perpendicular mirror hinging [44], [105]. The lower figure shows the shape of the out-of-phase torsion mode. The angular coupling ratio is 17 at the 39579 Hz resonance frequency. Reprinted with permission from [105].

C. Piezoelectrically Actuated Scanners

During the last decade several different actuation configurations for PE scanner have been tested. Smits et al. developed one of the first successful piezoelectric thin-film actuated resonant scanners in 2005, demonstrating 30° at 17.4 kHz [96]. The same year Filhol et al. introduced a novel actuator design with a working frequency of 25.4 kHz in ambient atmosphere consisting of a silicon membrane and a PZT film [92]. A circular mirror with 500 μm diameter is asymmetrically (50 μm off axis to the center of mass of the mirror) mounted on two lateral torsional hinges linked to the actuators so that the vertical translational excitation is converted into a rotational oscillatory movement of the mirror. In [106] the rotation is achieved by surrounding the rotation bar with two unimorph actuator beams supplied with opposite voltage. This method is illustrated in Fig. 6(b).

As already stated Section III-C the major problem to overcome for high angle PE scanners is the limited stroke length of the actuator. Baran et al. proposed a novel actuation scheme with a mechanically coupled indirect drive [44]. (See Section III-D for more discussion of the indirect drive.) The PZT film is deposited on the outer frame [Fig. 11(b)], so that the actuation is done within the moving structure itself. The 40 kHz device has an angular coupling ration of 17. To isolate the mirror and limit the mirror deformation the mirror is suspended by two flexures orthogonal to the torsion bars. This solution is a development of the mirror suspension used for the ES scanner presented in [85]. An improved version of the scanner with approximately 40% performance increase for corresponding voltage level was presented in [84]. The mechanical structure is identical, but the PZT electrode is tailored to have a static deflection profile that conforms with the desired eigenmode shape. This change decreases the power with 23% for a fixed voltage level. At 25V an angle of 54.4° is achieved, leading to a $\theta_{opt} \cdot D$ of *76.3* deg·mm and a $\theta_{opt} \cdot D \cdot f$ of 3052 deg·mm·kHz. This is the so far the highest fast scanner performance in the literature. In 2013 Gu-Stoppel et al. presented a single-axis scanner actuated with thin-film PZT. The 1 mm mirror scans resonantly $\pm 10.6°$ at 32 kHz [95]. It uses an indirect drive to increase the deflection. This work and the scanner presented by Baran et al. show that PE scanners in combination with the indirect drive can reach higher $\theta_{opt} \cdot D \cdot f$−numbers than competing technologies.

Metal based piezoelectric scanners have also been investigated. Park et al. introduced a stainless steel based piezoelectric scanner operating at 28.24 kHz [88]. Moreover, Matsushita et al. developed a 25.4 kHz PZT film actuated scanner on a Ti substrate to simplify the fabrication process of piezoelectric thin film MEMS [91]. Both these metal-based scanners showed good control of dynamic deformation.

An alternative to PE film is the use of PE bulk elements. Iseki et al. demonstrated a large rotation of $\pm 27°$ optical scan angle at 38 kHz with 1 mm mirror using a stack piezoelectric actuator [89]. In an attempt to get around the material limitations of silicon Desai et al. from Cornell University proposed in 2006 a hybrid solution where a silicon mirror is suspended by carbon fiber flexures [64]. With the traditional silicon flexures replaced by the much more elastic carbon fiber the fatigue limitations eased considerably. The device is actuated with an external piezo drive that makes very large scan angles possible. Optical angles greater than 180° at 2.5 kHz are reported. What this hybrid technology does not solve is dynamic deformation of the mirror, which often is the most difficult problem to solve for high frequency scanners. Development of the technology is continued by Mezmeriz Inc.

V. Non-Resonant Scanners (Slow Axis)

Polygon and galvanometric scanners with closed-loop control are widely used in various laser-scanning applications

and provide an excellent linear scan, but are bulky. While much research interest has been directed towards resonant high frequency scanners, the requirements for the slow axis scanners are at least as difficult to meet. Typical requirements are 60 Hz operation frequency and a saw tooth scan waveform, capable of constant velocity during the forward scan and fast retrace time for the backward scan. The constant velocity provides even spacing between the raster lines and the fast retrace time maximizes the fraction of the time used for writing pixels, thus minimizing the frequency requirement for the fast axis scanner and the display brightness as lasers are turned off during the retrace. Since MEMS scanners are suspended mirrors connected to a frame with torsional flexures, their dynamic behavior can be modeled as a simple spring, mass, damper system. Under ambient operation conditions, they are under damped ($Q \gg 1$) and exhibit resonance behavior. As a result, the constant speed and fast retrace requirements make it a challenging design and control problem.

In actual applications the operation frequency of the slow axis is kept close to the incoming video frame rate (typically 60Hz), but not constant. Instead it will be made to vary with the changes in the resonance frequency of the fast axis scanner. There should be an integer ratio between the two axis frequencies in a master-slave configuration to produce a stationary raster pattern. Due to the large number of harmonics present in a saw tooth scan waveform, the slow axis scanner dynamics as well as the changes in the dynamics of both axes due to temperature shifts need to be taken into account when designing the excitation waveform [107].

While raster scanning is the most common approach, so called Lissajous scanning with two resonant axes has also been demonstrated. The main advantages with this approach come with the driving requirements for the slow axis due to absence of harmonics [45], [51], [108]. The power consumption is also somewhat smaller. On the negative side, the raster lines are not evenly spaced and correcting this leads to complicated electronics and an increase of the required horizontal frequency. Even when this requirement is fulfilled the resulting refresh rate is lower than for a comparable raster scanning system. Bi-resonant actuation also demands larger electronic bandwidth. For the best coverage in a Lissajous system a high ratio between the two resonant axes is desired. This requires the slow scanner to work resonantly at very low frequencies, which makes the system very fragile and sensitive to vibrations. In [45] this is addressed by a proposed setup where two fast scanners are paired. The two axes are individually monitored by phase-locked loop circuitry (PLL) to keep the difference between the two working frequencies at exactly 60 Hz. In this way you get a rather robust system, but one that is not aiming at high end applications. The common assumption in the literature is that Lissajous scanners are not well-suited for high quality displays, but probably more so for imaging applications where a feedback signal together with data processing can reconstruct the a high resolution image. There are examples of successful use of Lissajous scanners in endoscopic and confocal microscopy applications [4]. For more in-depth discussions of Lissajous scanning the authors refer to the following references [45], [109]–[111].

TABLE IV
HIGH PERFORMING NON-RESONANT SCANNERS. AVC: ANGULAR VERTICAL COMBS. SVC: STAGGERED VERTICAL COMBS

Actuation	θ_{opt} [deg]	D [mm]	$\theta_{opt}\cdot D$ [deg·mm]	Mechanical Design	Notes and Reference
ES, Comb Drive	30	4	120	SVC, 1D	AVC and SVC with similar performance are shown. [94]
ES, Comb Drive	30	1.2	36	SVC, 2D	See entry above. [94]
ES, Comb Drive	39	-	-	Multilevel Comb Drive.	Technology demonstration showing capability of tip-tilt-piston actuators. [112]
EM, Moving Coil	65	1.5	97.5	2D	Non-resonant scanning from dc to 2 kHz possible. [38]
PE, PZT Film	29	1.5	43.5	Meander Spring, 2D	60 Hz working frequency. [78]

Only a few quasistatic scanners with high θ_{opt} are found in the literature, but is has been well demonstrated that this can be done for ES [94], [112], [113] and EM [38], [114] scanners. For PE scanners some very good progress has been made, but more work remains to be done [68]. In this section non-resonant 1D scanners are mainly discussed, see Section VI for those included in 2D scanners. For a better overview some of the highest performing non-resonant scanners in the literature are collected in Table IV.

A. Electrostatically Actuated Scanners

To facilitate quasistatic ES scanning it is necessary to have a vertical separation (off-set) between the moving and static electrodes. For comb drive actuators the two most important approaches are staggered vertical combs (SVC) and the angular vertical combs (AVC). The earliest SVC scanner used partial polysilicon refill of vertical trenches to form the comb fingers [55]. The straightforward way to fabricate these nowadays is to form the two finger sets in separate device layers in an SOI wafer [43], [112]. Two drawbacks shared by most SVC fabrication schemes are the complicated fabrication schemes and the fact that the static and moving finger sets are defined with separate mask, leading to very strict alignment requirements. To address the latter point several methods to fabricate so called self-aligned comb drives, where all fingers are defined with one mask, have been developed [113], [115], [116]. However, these solutions increase the complexity even more. In their 2004 paper Milanovic et al. presented a scanner where timed etches are used to create all comb sets from the same silicon layer [97]. They report a gimbal-less micromirror [Fig. 9(a)] actuated by three or four vertical comb drive rotators. These rotators are coupled through mechanical rotation transformers to a central mirror. The one-axis micromirror is capable of angles above $\pm 5°$ when operated below 150 V operation. Devices with three or four rotators have three degrees of freedom (tip-tilt-piston). In 2002 Milanovic demonstrated a scanner with an SOI-based fabrication schedule with an optical angle of $\pm 19.5°$ [112]. Carlen et al. presented several SVC devices with $\pm 10°$ optical angle [113].

In AVC devices static and moving fingers are typically defined in one layer with one mask. This removes much of the fabrication complexity of SVC devices. In the next step a static offset angle is created. Many techniques have been presented to achieve this offset, among them are stress induced bending in multilayered joints [117], surface-tension forces from reflow of photoresist [118], or plastic deformation of silicon through annealing [119]. It has also been shown AVC actuators are more efficient than SVC for the same finger geometry [118].

Researchers at Fraunhofer IPMS (FhG-IPMS) presented scanners with out-of-plane combs constructed by deforming in-plane combs during a wafer bonding step between the mirror wafer and a cover wafer [94]. During the bonding step so called solid body mechanisms on the scanner wafers are deflected by stamp structures on the cover wafer [Fig. 9(e)]. Both AVC and SVC structures are fabricated with this technique. The main difficulty with this fabrication scheme is to reach the acquired lateral resolution in the wafer bonding step. The authors report a maximum lateral displacement of ± 0.6 μm. See also Section VI-A.

As an alternative, in-plane rotation using curved comb fingers can also be used to drive scanning platforms for laser scanning applications. In [120] such a mechanism was used to rotate a 1 mm in-plane grating for monochrome scanning up to 25° at resonance. One problem with in-plane MEMS scanners using tether suspensions is the nonlinear spring stiffening of suspension beams used in bending mode rather than torsion mode [121]. An ES rotating platform utilizing a suspension geometry designed to provide a linear ramp motion with a vertically mounted mirror was demonstrated in [53].

B. Electromagnetically Actuated Scanners

There are several successful examples of electromagnetically actuated non-resonant MEMS laser scanners. Less nonlinear drive and longer operation range capabilities of EM actuators make them suitable for quasistatic operation. Jeong et al. from Samsung Electrics Company, Ltd. proposed a Lorentz force slow scanner that can be used to horizontally scan a vertical line image made through a line-type diffractive SLM [122]. In this design a large 3×1.5 mm^2 mirror is rotated quasistatically up to $\pm 15°$ with 98% linearity at 120 Hz, while consuming 60 mW. To minimize the device size and the power consumption the coil actuator is placed directly on the reverse of the mirror. Moreover, mechanical stoppers are used to make the device shock-proof. Wafer-level packaging is realized using an additional glass wafer, and total size of the package is 9.2 mm $\times$ 10 mm $\times$ 3 mm (0.28cc).

Moreover, Makishi et al. uses moving magnet actuation to generate very large mirror rotations up to $\pm 59°$ optical angle [114]. Four permanent magnets are attached to a double-gimbal structure and the mirror rotation is realized with four electromagnets. The possible unreported problems with this device are large size due to the bulky electromagnets and poor shock resistance. Permanent magnets add comparably large amount of inertia to the double-gimbal structure and makes it easier to break under shock.

Ataman et al. presented a non-gimbaled 2D moving magnet pointing mirror for use with high power lasers [18]. The mirror is suspended by 25 hidden and radially symmetric s-shaped beams. A magnet is attached to the mirror below the pivot point. The mirror can be mechanically tilted $\pm 4°$ ($\pm 8°$ optical) along both axes by current applied to two coils, stacked beneath the mirror.

C. Piezoelectrically Actuated Scanners

The limited displacement of piezoelectric actuation is a major problem for non-resonant MEMS scanners. Hence, there are few examples of non-resonant MEMS scanners with piezoelectric actuation in literature. Tani et al. introduced a solution to overcome the limited deflection of piezoelectrically actuated beams [68], [123]. In this design large quasistatically actuated angles up to $\pm 17.2°$ are achieved at an applied voltage of 20 V_{dc} by accumulating angular displacement in a meandering piezoelectric cantilever, as illustrated in Fig. 11(a). Kobayashi et al. used meandering cantilevers to create large, non-resonant angle rotation of a mirror [124]. In this way, $\pm 10.6°$ at an applied voltage of 10 V_{dc} is achieved.

Meandering type cantilevers are known to have a problem with an abundance of parasitic modes at the typically desired low frequencies, making it a challenge to achieve linear scanning that is pure enough for high performance displays. The approach suggested by Tani et al. for quasistatic PE scanning is, however, clearly the most promising so far, but much work on detailed mode design will probably be required to get this type of scanner to work with the precision needed.

VI. 2D Scanners

The first silicon 2D MEMS scanner was published already in 1994 by Asada et al. [125]. Most high performance dual axis scanners for display applications use a gimbaled torsion mechanism. However, several gimbal-less approaches have been demonstrated. Scanners with the actuation mechanics hidden beneath the mirror are especially important for applications that require very small die size or high mirror fill-factor [18], [48], [126]. A non-gimbal approach was also used in the tip-tilt-piston mirror presented by Milanovic et al. [97].

A few hybrid approaches to 2D scanning have been published. Already a decade ago Microvision made an ES/EM 2D scanner. The device required a vacuum package and utilized EM actuation for a slow raster scan and ES parallel plate drive for resonant fast scanning [30]. A distinct possibility for hybrid 2D scanners is ET actuation. Successful 2D scanning ET micromirrors have been presented [48], but it is inherent to the actuation principle that the reaction times are too long to be used for the fast axis in a display. To function for this purpose a slow ET actuator would need to be paired with a different actuation scheme for the fast axis. 2D ET scanners using ES and EM, respectively, for the fast axis have been reported [49], [50], but it remains to be proven if it is a viable idea or not.

A. Electrostatically Actuated Scanners

The 2D ES microscanner is a very good candidate for miniaturized laser projectors, the main drawback being the

high voltage requirements typically needed. FhG-IPMS has been developing electrostatically actuated MEMS scanners for over a decade [87], [127]. Much of the work has been on 2D scanners for microdisplays utilizing Lissajous scanning (see Section II and the introduction of V) [51], [94], [108]. In 2008 they presented the first 2D ES scanner capable of SVGA resolution [108]. The gimbaled scanner uses a fast axis frequency of 30 kHz and a slow axis of either 70Hz or 330Hz. The design of the fast axis is the same as in [87], previously discussed in Section IV-A. The dynamic deformation is established to be within the optical requirements. The high frequency of the fast axis is needed for SVGA because of the Lissajous scheme. The required frequency for the corresponding raster scanner would be around 20 kHz. In 2011 researchers at FhG-IPMS presented newly developed dual-axis micromirrors capable of performing high frequency resonant scanning as well as linear quasistatic scanning [94]. For the quasistatic slow axis both SVC and AVC configurations are been realized (see Section V-A). The fast axis scans up to ±19° at 23.3 kHz, while the presented quasistatic axes give optical scan angles up to ±15°. The 2D scanners have mirrors with 1.2 mm in diameter. Pure slow scanners with mirror diameter of 4 mm are also presented.

Hofmann et al. reported several ultra-high Q 2D scanners for Lissajous operation in vacuum [45]. One of the four presented designs reaches ±43° at 30.8 kHz. The approach used is to lower the voltage requirements for high performance scanners by way of very high Q of 145,000 for the slow axis and 60,000 for the fast axis. To achieve this wafer level vacuum packaging is used. With a 0.8 mm mirror this gives a $\theta_{OPT} \cdot D = 68.8$ deg·mm and a $\theta_{OPT} \cdot D \cdot f = 2119$ deg·mm·kHz. The power consumption is below 1 mW with both axes running. These are the highest performance metrics for an ES fast scanner to date. When operating in ambient atmosphere the scan angle is about one tenth of these values. The drawbacks with the high Q are extremely long amplitude decay times (minutes), high sensitivity of the resonance frequency to temperature changes, and when both axes have extremely high Q the synchronisation of them becomes very difficult.

Chu et al. reported two bi-resonant, gimbaled 2-D comb drive scanners, using direct drive for both axes [Fig. 9(d)] [81]. One of the scanners exhibit resonant frequencies for the inner mirrors and the gimbal frame of 40 kHz and 162 Hz, respectively. The maximum scan angle for the fast axis is ±10.8° operating at 1 Pa. At ambient pressure the performance is limited. Researchers from the Adriatic Research Institute presented in [128] a projection systems based on their non-gimbaled 2D scanners [97], described in Section V-A. The mirror can rotate mechanically up to ±4° on each axis, but with an added fisheye lens the optical angle can reach 120°. Both axes can be actuated linearly at arbitrary frequencies up to 4 kHz, making it especially suitable for vector displays.

B. Electromagnetically Actuated Scanners

2D EM laser scanners are core components of commercially available mobile projectors [30], [39]. Microvision Inc. has been utilizing Lorentz force excited 2D MEMS scanners as an engine for their NOMAD head-worn displays and PicoP mobile projectors [30], [38], [46]. Early designs required a vacuum package, significantly increasing size and cost. In 2005 this approach was replaced by a new bi-axial magnetic drive scheme to be used in ambient atmosphere [46]. The scheme was detailed in 2006 by Yalcinkaya et al. and the featured scanner was the first SVGA capable 2D raster scanner, see Fig. 10(a) [38]. The 1.5 mm mirror gives optical angles up to ±26.5° and ±33.5° at resonant horizontal scan at 21.3 kHz and non-resonant vertical scan at 60 Hz, respectively. The scanner utilizes Lorentz force actuation. For actuation the device is placed in an external magnetic field, at a 45° angle, allowing both modes to be actuated simultaneously by super positioning of two driving signals in the coil covering the gimbal frame. For the resonant scan the out-of-phase mode is used to benefit from mechanical coupling.

An interesting addition to the literature on Lorentz scanners was presented by Sung et al. in [129]. The authors note that in a traditional Lorentz scanner like the one by Yalcinkaya et al. where the coil is deposited on the silicon surface there will be a slight asymmetry in the actuation, leading to a wobble motion. In this work the wobble motion is minimized by the use of a Si-Ni compound frame, where the Ni coil spans through the full thickness of the scanner.

Ji et al. presented a scanner that again uses the mechanical coupling principle for resonant scanning, but it utilizes a single turn coil and radial magnetic field from concentric magnet assembly rather than using a multi turn coil and a lateral magnetic field oriented 45° to the scan axes to achieve a bi-axial magnetic actuation, see Fig. 10(b) [72]. A single turn coil is easier to fabricate than a multi turn coil. A concentric magnet assembly, composed of cylindrical and annular magnets and an iron yoke, provides larger radial magnetic field compared against the conventional magnets. In this design, 1.5 mm mirror operating with 131 mA current produces 8.8° and 8.3° optical scan angles in resonance operation at 19.1 kHz, and in static mode operation at 60 Hz, respectively.

C. Piezoelectrically Actuated Scanners

While there have been several examples of biresonant PE 2D scanners, it has proven to be very difficult to design a high performance dual-axis scanner for raster scanning [93], [106], [130]. Chen et al. presented in 2012 a 2D Lissajous scanner driven by an external PZT unit [93]. The resonance frequencies of axes are 25 kHz and 560 Hz, respectively and projects images with a 640 × 480 resolution. Gu-Stoppel et al. presented a gimbal-less stage with three degrees of freedom granted by four PZT-clad cantilevers [131]. The torsion modes resonate at 28.6 kHz and the piston mode at 21 kHz.

The meander spring presented by Tani et al. is described above in Section V-C. These springs can be actuated either quasistatically or at resonance. A scanner using the meander spring for both axes was presented in [123]. Non-resonant optical angles of ±17.2° and ±11.2° were found for the outer and inner axes, respectively. Separately, a hybrid scanner was created where a meandering slow outer axis is combined with a more traditional torsion beam twisted by two unimorph beams

for a fast inner axis [68]. The scanner is shown in Fig. 11(a). In this work, 2D scan is demonstrated with a resonant operation at 11.2 kHz for the fast horizontal axis with 39° optical angle and quasistatic operation at 60 Hz of the slow vertical axis with ±7.25° while operated at 40 V_{pp}. With that it is the first successful demonstration of a piezoelectrically actuated raster scanner in the literature.

VII. Discussion and Conclusion

A. Fabrication and Packaging

The processes of MEMS fabrication are derived from the very mature semiconductor IC industry. While the MEMS field still lack standardization compared to the IC industry, the MEMS industry is maturing rapidly with greater standardization as one inevitable result. We have already seen thick SOI based wafers with device layer thickness in the range of 30 μm to 150 μm becoming the standard substrate for scanners, leading to simple and robust structures. As shown in Fig. 8, all three actuation principles reviewed in this paper can produce high performance scanners. One disadvantage for magnetically actuated scanners is the cost and volume taken up by the required magnets. They also require good shielding for magnetic interference. From a manufacturing point-of-view, all three types can use standard materials and fabrication methods. While some of the early MEMS scanners exploited the use of expensive vacuum packaging, of more recently reported high-performance scanners most operate at ambient pressure and do not have special packaging requirements.

B. Economies of Scale

The die area primarily determines the cost of the scanners in high volume production. Increasing the resolution by way of increasing the scan angle does not increase the scanner cost and allows scalability to higher resolutions. While the scanner cost is important, the cost of the system is dominated by the lasers not by the scanners in display and imaging devices. Power consumption per scan axis can be less than 100 mW for all types of scanners. While the power consumption of EM actuated scanners is higher, the system power consumption is dominated by the lasers and the video electronics rather than by the scanners.

C. Technology Comparison for Miniaturized Displays

For microdisplay applications, major competitors to laser scanning are DLP and LCOS based systems that use LEDs as light source. Key advantages of the laser scanners for mobile projection displays are in the scaling to higher resolutions and focus-free operation without requiring a projection lens. From an economic perspective chips for laser scanning are simpler to fabricate and smaller in die area, thus cost less. One drawback of the laser-based systems is speckle, which degrades the image quality. However, there are various methods to reduce the speckle contrast to acceptable levels in laser displays [31]. Both LED and laser based mobile displays are currently limited in brightness due to eye safety and battery power limitations. However, novel screen designs with high-gain can offer high-efficiency, high-brightness and a new found flexibility for 2D and 3D projection displays [132], [133].

D. Commercialization trends for displays

The field has already reached some maturity and there are already commercial offerings with a wide variety of technical solutions for high performance MEMS laser scanners. The first product in the market was Microvision NOMAD in 2004, which used a 2D scanner with parallel-plate ES scanner for fast axis and moving coil EM scanner for slow axis. Later products of Microvision used 2D EM scanners and more recently Lemoptix SA and Nippon Signal also offer both 1D and 2D EM scanners. Fraunhofer IPMS (and its spin-off Hyperscan GmbH), Mirrorcle Technologies, and Opus Microsystems (1D and 2D ES) have been offering 1D and 2D ES scanners . There are also some more unusual approaches such as the 2D scanner from Maradin Ltd. with an ES fast scanner and moving magnet slow scanner and the hybrid PE solution from Mezmeriz Inc (see Section IV-C for more detail of the latter). There are other companies such as Stanley and BTendo (acquired by STMicroelectronics) who developed scanners for commercialization but details are not available.

E. Roadmap for Medical Imaging Applications

There is much interest for miniaturized imaging solutions based on laser scanning in the medical field. The speed and the resolution of the camera based systems are typically determined by camera refresh rate and light source/optics while the scanning based systems are often limited by the low signal levels collected from the samples, which limit the bandwidth of detection and the scanning speed. Additional requirements in medical imaging applications are micron level small spot size, large field-of-view (or scan angle), and dynamic focusing due to limited depth-of-focus, which present major challenges in the optical design. For the scanning unit, $<$2 kHz scanning frequency for the fast axis and a high precision ramp scanning in the slow axis are preferred. Galvo scanners have been dominating the scanner market for imaging applications due to their superior linearity and stability up to 1 kHz scanning frequency. However, the efforts for miniaturizing the scanning unit, especially for endoscopic applications, generated a substantial literature about MEMS scanners for imaging applications. The performance requirements on MEMS scanners for imaging applications typically are much lower in terms of frequency and scan angle compared to those of in the display field and the challenges are more related to packaging. Good summaries of these scanners can be found in [134] and [135]. The main challenges for MEMS scanners developed for endoscopic imaging applications are compact package size requirement (preferably $<$10 mm^3), poor image quality (due to aberrations from scanning mirror and objective lens), and stability. These challenges have to be overcome to enable the implementation of MEMS scanners into commercial imaging systems. EM actuators fail to deliver compact package size due to their need for a bulky magnet. On the other hand, ES and PE actuated MEMS scanners are closer candidates to satisfy the requirements of endoscopic imaging applications, however

significant engineering effort is still needed to limit optical aberrations and to control scanner stability.

In conclusion, we can assert that MEMS laser scanner based display and imaging systems offer several clear advantages and expected to have a bright future particularly in mobile consumer displays and medical imaging devices.

Acknowledgment

The authors would like to thank Microvision Inc. for our longstanding collaboration, special thanks to Dean Brown, Wyatt Davis, Mark Helsel, and Randy Sprague for countless fruitful discussions on these topics. For help with technology development the authors would also like to thank Paul Muralt and Davide Balma from École Polytechnique Fédérale de Lausanne and Harald Schenk from Fraunhofer IPMS. Also many thanks to present and former colleagues at OML: Arda Yalcinkaya, Caglar Ataman, Aslihan Arslan, Sertan Kutal Gokce, Selim Olcer, Basarbatu Can, and Ugur Aygun.

References

[1] K. E. Petersen, "Silicon torsional scanning mirror," *IBM J. Res. Develop.*, vol. 24, no. 5, pp. 631–637, 1980.

[2] D. Dickensheets and G. Kino, "Micromachined scanning confocal optical microscope," *Opt. Lett.*, vol. 21, no. 10, pp. 764–766, May 1996.

[3] W. Piyawattanametha, H. Ra, M. J. Mandella, K. Loewke, T. D. Wang, G. S. Kino, *et al.*, "3-D near-infrared fluorescence imaging using an MEMS-based miniature dual-axis confocal microscope," *IEEE J. Sel. Topics Quantum Electron.*, vol. 15, no. 5, pp. 1344–1350, Sep. 2009.

[4] J. T. C. Liu, N. O. Loewke, H. Ra, O. Solgaard, C. H. Contag, G. S. Kino, *et al.*, "Micromirror-scanned dual-axis confocal microscope utilizing a gradient-index relay lens for image guidance during brain surgery," *J. Biomed. Opt.*, vol. 15, no. 2, pp. 026029-1–026029-5, 2010.

[5] K. H. Gilchrist, D. E. Dausch, and S. Grego, "Electromechanical performance of piezoelectric scanning mirrors for medical endoscopy," *Sens. Actuators A, Phys.*, vol. 178, pp. 193–201, Apr. 2012.

[6] D. L. Dickensheets, "A microfabricated scanning confocal optical microscope for in situ imaging," Ph.D. dissertation, Dept. Elect. Eng., Stanford Univ., Stanford, CA, USA, 1998.

[7] D. L. Dickensheets and G. S. Kino, "Silicon-micromachined scanning confocal optical microscope," *J. Microelectromech. Syst.*, vol. 7, no. 1, pp. 38–47, Mar. 1998.

[8] S. O. Isikman, R. B. Sprague, and H. Urey, "FR4 laser scanner with dynamic focus," *IEEE Photon. Technol. Lett.*, vol. 21, no. 4, pp. 233–235, Feb. 15, 2009.

[9] A. P. Neukermans and T. G. Slater, "Micromachined torsional scanner," U.S. Patent 5 629 790, May 13, 1997.

[10] V. A. Aksyuk, F. Pardo, C. A. Bolle, S. Arney, C. R. Giles, and D. J. Bishop, "Lucent microstar micromirror array technology for large optical crossconnects," *Proc. SPIE*, vol. 4178, pp. 320–324, Aug. 2000.

[11] P. R. Patterson, D. Hah, M. Fujino, W. Piyawattanametha, and M. C. Wu, "Scanning micromirrors: An overview," *Proc. SPIE*, vol. 5604, pp. 195–207, Oct. 2004.

[12] Y. Pan, H. Xie, and G. K. Fedder, "Endoscopic optical coherence tomography based on a microelectromechanical mirror," *Opt. Lett.*, vol. 26, no. 24, pp. 1966–1968, Dec. 2001.

[13] K. Isamoto, K. Totsuka, T. Suzuki, T. Sakai, A. Morosawa, C. Chong, *et al.*, "A high speed MEMS scanner for 140-kHz SS-OCT," in *Proc. IEEE Opt. MEMS*, Istanbul, Turkey, Aug. 2011, pp. 73–74.

[14] H. Urey, D. W. Wine, and J. R. Lewis, "Scanner design and resolution tradeoffs for miniature scanning displays," *Proc. SPIE*, vol. 3636, pp. 60–68, Apr. 1999.

[15] W. O. Davis, D. Brown, M. Helsel, R. Sprague, G. Gibson, A. Yalcinkaya, *et al.*, "High-performance silicon scanning mirror for laser printing," *Proc. SPIE*, vol. 6466, pp. 64660D-1–64660D-7, Jan. 2007.

[16] M. K. Hedili, M. O. Freeman, and H. Urey, "Microstructured head-up display screen for automotive applications," *Proc. SPIE*, vol. 8428, pp. 84280X-1–84280X-6, Jun. 2012.

[17] U. Hofmann, F. Senger, F. Soerensen, V. Stenchly, B. Jensen, and J. Janes, "Biaxial resonant 7 mm-MEMS mirror for automotive LIDAR application," in *Proc. Int. Conf. Opt. MEMS Nanophoton.*, Banff, AB, Canada, 2012, pp. 150–151.

[18] Ç. Ataman, S. Lani, W. Noell, and N. de Rooij, "A dual-axis pointing mirror with moving-magnet actuation," *J. Microelectromech. Syst.*, vol. 23, no. 2, p. 025002, Dec. 2012.

[19] L. J. Hornbeck, "The DMD projection display chip: A MEMS-based technology," *MRS Bull.*, vol. 26, no. 4, pp. 325–327, Apr. 2001.

[20] S. C. Shin, Y. Jung, T. J. Ahn, S. S. Jeong, S. G. Lee, and K. Y. Choi, "The compact systems design based on DMD and the straight line 2-channel LED for a mobile embedded pico projector," *J. Display Technol.*, vol. 8, no. 4, pp. 219–224, Apr. 2012.

[21] O. Solgaard, F. Sandejas, and D. Bloom, "Deformable grating optical modulator," *Opt. Lett.*, vol. 17, no. 9, pp. 688–690, May 1992.

[22] A. Londergan, E. Gousev, and C. Chui, "Advanced processes for MEMS-based displays," in *Proc. Asia Displays*, Shanghai, China, 2007, pp. 107–112.

[23] T. Bourouina, H. Fujita, G. Reyne, and M. E. Motamedi, "Optical scanning," in *Micro-Opto-Electro-Mechanical Systems*, M. E. Motamedi, Ed. Bellingham, WA, USA: SPIE, 2005, pp. 323–367.

[24] H. Urey, S. Madhavan, and M. Brown, "MEMS microdisplays," in *Handbook of Visual Display Technology*, J. Chen, W. Cranton, and M. Fihn, Eds. Bristol, U.K.: Springer-Verlag, 2012, pp. 2067–2080.

[25] A. Korpel, R. Adler, P. Desmares, and W. Watson, "A television display using acoustic deflection and modulation of coherent light," *Appl. Opt.*, vol. 5, no. 10, pp. 1667–1675, Oct. 1966.

[26] H. Urey, D. W. Wine, and T. D. Osborn, "Optical performance requirements for MEMS-scanner based microdisplays," *Proc. SPIE*, vol. 4178, pp. 176–185, Aug. 2000.

[27] K. Yamada and T. Kuriyama, "A novel asymmetric silicon micro-mirror for optical beam scanning display," in *Proc. 11th Annu. IEEE Micro Electro Mech. Syst.*, Kanagawa, Japan, Jan. 1998, pp. 110–115.

[28] R. A. Conant, P. M. Hagelin, U. Krishnamoorthy, M. Hart, O. Solgaard, K. Y. Lau, *et al.*, "A raster-scanning full-motion video display using polysilicon micromachined mirrors," *Sens. Actuators A, Phys.*, vol. 83, pp. 291–296, May 2000.

[29] H. Schenk, "A novel micro actuator for one and two dimensional deflection of light," Ph.D. dissertation, Dept. Elect. Eng., Gerhard Mercator Univ., Duisburg, Germany, 2000.

[30] J. Tauscher, W. O. Davis, D. Brown, M. Ellis, Y. Ma, M. E. Sherwood, *et al.*, "Evolution of MEMS scanning mirrors for laser projection in compact consumer electronics," *Proc. SPIE*, vol. 7594, pp. 75940A-1–75940A-12, Feb. 2010.

[31] K. V. Chellappan, E. Erden, and H. Urey, "Laser-based displays: A review," *Appl. Opt.*, vol. 49, no. 25, pp. F79–F98, Sep. 2010.

[32] Y. Hirano, S. Yamamoto, Y. Akino, A. Nakamura, T. Yagi, H. Sugiura, *et al.*, "High performance micro green laser for laser TV," in *Proc. Adv. Solid-State Photon.*, Denver, CO, USA, 2009, pp. 1–3.

[33] S. J. Park, S. M. Kim, and C. S. Won, "Design considerations for pico-projector based on LCoS and 3-LEDs," in *Proc. IEEE Consumer Electron.*, Las Vegas, NV, USA, Jan. 2011, pp. 805–806.

[34] W. O. Davis, M. Beard, and R. Jackson, "Trajectory precision of micromachined scanning mirrors for laser beam scanning pico-projector displays," *Proc. SPIE*, vol. 8252, pp. 825203-1–825203-11, Mar. 2012.

[35] M. Freeman, M. Champion, and S. Madhavan, "Scanned laser pico-projectors: Seeing the big picture (with a small device)," *Opt. Photon. News*, vol. 20, no. 5, pp. 28–34, May 2009.

[36] C. Liao and J. Tsai, "The evolution of MEMS displays," *IEEE Trans. Ind. Electron.*, vol. 56, no. 4, pp. 1057–1065, Apr. 2009.

[37] M. C. Wu, O. Solgaard, and J. E. Ford, "Optical MEMS for lightwave communication," *J. Lightw. Technol.*, vol. 24, no. 12, pp. 4433–4454, Jan. 2006.

[38] A. D. Yalcinkaya, H. Urey, D. Brown, T. Montague, and R. Sprague, "Two-axis electromagnetic microscanner for high resolution displays," *J. Microelectromech. Syst.*, vol. 15, no. 4, pp. 786–794, Aug. 2006.

[39] D. Raboud, T. Barrasa, F. Lo Contea, L. Fabrea, L. Kilcherb, F. Kechanab, *et al.*, "MEMS based color-VGA micro-projector system," *Proc. Eng.*, vol. 5, pp. 260–263, Sep. 2010.

[40] H. Urey, "Torsional MEMS scanner design for high-resolution display systems," *Proc. SPIE*, vol. 4773, pp. 27–37, Jun. 2002.

[41] K. D. Powell, H. Urey, and M. M. Bayer, "Multibeam bidirectional raster scanning in retinal scanning displays," *Proc. SPIE*, vol. 4361, pp. 77–88, Aug. 2001.

[42] P. Brosens, "Dynamic mirror distortions in optical scanning," *Appl. Opt.*, vol. 11, no. 12, pp. 2987–2989, Dec. 1972.

[43] R. A. Conant, J. T. Nee, K. Y. Lau, and R. S. Muller, "A flat high-frequency scanning micromirror," in *Proc. Solid-State Sens., Actuators Workshop*, Hilton Head Island, SC, USA, 2000, pp. 6–9.

[44] U. Baran, D. Brown, S. Holmstrom, D. Balma, W. O. Davis, P. Muralt, *et al.*, "Resonant PZT MEMS scanner for high-resolution displays," *J. Microelectromech. Syst.*, vol. 21, no. 6, pp. 1303–1310, Dec. 2012.

[45] U. Hofmann, J. Janes, and H. J. Quenzer, "High-Q MEMS Resonators for Laser Beam Scanning Displays," *Micromachines*, vol. 3, no. 2, pp. 509–528, Jun. 2012.

[46] R. B. Sprague, T. Montague, and D. Brown, "Bi-axial magnetic drive for scanned beam display mirrors," *Proc. SPIE*, vol. 5721, p. 1, Feb. 2005.

[47] Y. Xu, J. Singh, T. Selvaratnam, and N. Chen, "Two-axis gimbal-less electrothermal micromirror for large-angle circumferential scanning," *IEEE J. Sel. Topics Quantum Electron.*, vol. 15, no. 5, pp. 1432–1438, Sep. 2009.

[48] K. Jia, S. R. Samuelson, and H. Xie, "High-fill-factor micromirror array with hidden bimorph actuators and tip-tilt-piston capability," *J. Microelectromech. Syst.*, vol. 20, no. 3, pp. 573–582, Jun. 2011.

[49] K. H. Koh and C. Lee, "A low power 2-D raster scanning MEMS mirror driven by hybrid electrothermal and electromagnetic actuation mechanisms," in *Proc. IEEE Opt. MEMS Nanophoton.*, Banff, AB, Canada, Aug. 2012, pp. 236–237.

[50] L. Li, R. Bauer, G. Brown, and D. Uttamchandani, "A symmetric hybrid MEMS scanner with electrothermal and electrostatic actuators," in *Proc. IEEE Opt. MEMS Nanophoton.*, Istanbul, Turkey, Aug. 2011, pp. 163–164.

[51] H. Schenk, P. Dürr, D. Kunze, H. Lakner, and H. Kück, "A resonantly excited 2D-micro-scanning-mirror with large deflection," *Sens. Actuators A, Phys.*, vol. 89, no. 1, pp. 104–111, Mar. 2001.

[52] D. W. Wine, M. P. Helsel, L. Jenkins, H. Urey, and T. D. Osborn, "Performance of a biaxial MEMS-based scanner for microdisplay applications," *Proc. SPIE*, vol. 4178, pp. 186–196, Aug. 2000.

[53] U. Baran, W. Davis, S. Holmström, D. Brown, J. Sharma, S. Gokce, *et al.*, "Linear-stiffness rotary MEMS stage," *J. Microelectromech. Syst.*, vol. 21, no. 3, pp. 514–516, May 2012.

[54] W. C. Tang, T. C. H. Nguyen, M. W. Judy, and R. T. Howe, "Electrostatic-comb drive of lateral polysilicon resonators," *Sens. Actuators A, Phys.*, vol. 21, no. 1, pp. 328–331, Feb. 1990.

[55] A. Selvakumar, K. Najafi, W. H. Juan, and S. Pang, "Vertical comb array microactuators," in *Proc. IEEE MEMS*, Amsterdam, The Netherlands, Jan./Feb. 1995, pp. 43–48.

[56] E. S. Hung and S. D. Senturia, "Extending the travel range of analog-tuned electrostatic actuators," *J. Microelectromech. Syst.*, vol. 8, no. 4, pp. 497–505, Dec. 1999.

[57] Y. Nemirovsky and O. Bochobza-Degani, "A methodology and model for the pull-in parameters of electrostatic actuators," *J. Microelectromech. Syst.*, vol. 10, no. 4, pp. 601–615, Dec. 2001.

[58] G. N. Nielson and G. Barbastathis, "Dynamic pull-in of parallel-plate and torsional electrostatic MEMS actuators," *J. Microelectromech. Syst.*, vol. 15, no. 4, pp. 811–821, Aug. 2006.

[59] C. Ataman and H. Urey, "Modeling and characterization of comb-actuated resonant microscanners," *J. Micromech. Microeng.*, vol. 16, no. 1, pp. 9–16, 2006.

[60] K. L. Turner, S. A. Miller, P. G. Hartwell, N. C. MacDonald, S. H. Strogatz, and S. G. Adams, "Five parametric resonances in a microelectromechanical system," *Nature*, vol. 396, pp. 149–152, Nov. 1998.

[61] H. Urey, "MEMS scanners for display and imaging applications," *Proc. SPIE*, vol. 5604, pp. 218–219, Oct. 2004.

[62] J. Yan, S. Luanava, and V. Casasanta, "Magnetic actuation for MEMS scanners for retinal scanning displays," *Proc. SPIE*, vol. 4985, pp. 115–120, Jan. 2003.

[63] K. Uchino, "Piezoelectric actuators 2006," *J. Electroceram.*, vol. 20, pp. 301–311, Jul. 2008.

[64] S. Desai, A. Netravali, and M. Thompson, "Carbon fibers as a novel material for high-performance microelectromechanical systems (MEMS)," *J. Micromech. Microeng.*, vol. 16, no. 7, pp. 1403–1407, Jun. 2006.

[65] P. Muralt, "Piezoelectric thin films for MEMS," *Integr. Ferroelectr.*, vol. 17, no. 1, pp. 297–307, Aug. 1997.

[66] Y. Hishinuma, Y. Li, J. Birkmeyer, T. Fujii, T. Naono, and T. Arakawa, "High performance sputtered PZT film for MEMS applications," in *Proc. NSTI Nanotechnol. Conf.*, vol. 2. Santa Clara, CA, USA, 2012, pp. 137–140.

[67] P. Muralt, A. Kholkin, M. Kohli, and T. Maeder, "Piezoelectric actuation of PZT thin-film diaphragms at static and resonant conditions," *Sens. Actuators A, Phys.*, vol. 53, pp. 398–404, May 1996.

[68] M. Tani, M. Akamatsu, Y. Yasuda, H. Fujita, and H. Toshiyoshi, "A combination of fast resonant mode and slow static deflection of SOI-PZT actuators for MEMS image projection display," in *Proc. IEEE/LEOS Int. Conf. Opt. MEMS Appl. Conf.*, Big Sky, MT, USA, Aug. 2006, pp. 25–26.

[69] R. S. Fearing, "Powering 3 dimensional microrobots: Power density limitations," in *Proc. Tut. Micro Mech. Micro Robot., ICRA*, vol. 98. Sep. 1998, pp. 1–15.

[70] U. Baran, M. Tani, M. Akamatsu, Y. Yasuda, H. Fujita, and H. Toshiyoshi, "A built-in vibration sensor using arc-discharged reactive ion plated PZT," *IEEJ Trans. Sens. Micromach.*, vol. 131, no. 3, pp. 128–129, 2011.

[71] C. Lee, T. Itoh, T. Ohashi, R. Maeda, and T. Suga, "Development of a piezoelectric self-excitation and self-detection mechanism in PZT microcantilevers for dynamic scanning force microscopy in liquid," *J. Vac. Sci. Technol. B, Microelectron. Nanometer Struct.*, vol. 15, no. 4, pp. 1559–1563, Jul. 1997.

[72] C. H. Ji, M. Choi, S. C. Kim, K. C. Song, J. U. Bu, and H. J. Nam, "Electromagnetic two-dimensional scanner using radial magnetic field," *J. Microelectromech. Syst.*, vol. 16, no. 4, pp. 989–996, Aug. 2007.

[73] A. Arslan, D. Brown, W. O. Davis, S. Holmstrom, S. K. Gokce, and H. Urey, "Comb-actuated resonant torsional microscanner with mechanical amplification," *J. Microelectromech. Syst.*, vol. 19, no. 4, pp. 936–943, Aug. 2010.

[74] M. Yoda, K. Isamoto, C. Chong, H. Ito, A. Murata, S. Kamisuki, *et al.*, "A MEMS 1D optical scanner for laser projection display using self-assembled vertical combs and scan-angle magnifying mechanism," in *IEEE 13th Int. Conf. Solid-State Sensors, Actuat. Microsyst., Dig. Tech. Papers*, Seoul, Korea, Jun. 2005, pp. 968–971.

[75] S. Kurth, C. Kaufmann, R. Hahn, J. Mehner, W. Doetzel, and T. Gessner, "A novel 24-kHz resonant scanner for high-resolution laser display," *Proc. SPIE*, vol. 5721, pp. 23–33, Feb. 2005.

[76] A. D. Yalcinkaya, H. Urey, and S. Holmstrom, "NiFe plated biaxial MEMS scanner for 2-D imaging," *IEEE Photon. Technol. Lett.*, vol. 19, no. 5, pp. 330–332, Mar. 1, 2007.

[77] J. W. Cho, Y. H. Park, Y. C. Ko, B. L. Lee, S. J. Kang, S. W. Chung, *et al.*, "Electrostatic 1D microscanner with vertical combs for HD resolution display," *Proc. SPIE*, vol. 6466, pp. 64660B-1–64660B-12, Jan. 2007.

[78] A. Kuijpers, D. Lierop, R. Sanders, J. Tangenberg, H. Moddejonge, J. Eikenbroek, *et al.*, "Towards embedded control for resonant scanning MEMS micromirror," *Proc. Chem.*, vol. 1, no. 1, pp. 1307–1310, 2009.

[79] Y. C. Ko, J. W. Cho, Y. K. Mun, H. G. Jeong, W. K. Choi, J. W. Kim, *et al.*, "Eye-type scanning mirror with dual vertical combs for laser display," *Sens. Actuators A, Phys.*, vol. 126, no. 1, pp. 218–226, 2006.

[80] C. H. Ji, M. Choi, S. C. Kim, S. H. Lee, S. H. Kim, Y. Yee, *et al.*, "An electrostatic scanning micromirror with diaphragm mirror plate and diamond-shaped reinforcement frame," *J. Micromech. Microeng.*, vol. 16, no. 5, pp. 1033–1039, Apr. 2006.

[81] H. M. Chu and K. Hane, "Design, fabrication and vacuum operation characteristics of two-dimensional comb-drive micro-scanner," *Sens. Actuators A, Phys.*, vol. 165, no. 2, pp. 422–430, Feb. 2011.

[82] H. Noge, Y. Hagihara, K. Kawano, H. Ueda, and T. Yoshihara, "Electrostatically actuated two-dimensional optical scanner having a high resonant frequency ratio of fast/slow axes," *IEICE Trans. Electron.*, vol. 91, no. 10, pp. 1611–1615, Oct. 2008.

[83] T. Sandner, T. Klose, A. Wolter, H. Schenk, H. K. Lakner, and W. Davis, "Damping analysis and measurement for a comb-drive scanning mirror," *Proc. SPIE*, vol. 5455, pp. 147–158, Aug. 2004.

[84] H. Urey, S. Holmstrom, U. Baran, K. Aksit, M. K. Hedili, and O. Eldes, "MEMS scanners and emerging 3D and interactive augmented reality display applications," in *Proc. 17th Int. Conf. Solid-State Sensors, Actuat. Microsyst. Transducers Eurosensors*, Barcelona, Spain, Jun. 2013, pp. 2485–2488.

[85] S. K. Gokce, S. Holmstrom, D. Brown, W. O. Davis, and H. Urey, "A high-frequency comb-actuated resonant MEMS scanner for microdisplays," in *Proc. Int. Conf. Opt. MEMS Nanophoton.*, Istanbul, Turkey, Aug. 2011, pp. 35–36.

[86] K. Torashima, T. Teshima, Y. Mizoguchi, S. Yasuda, T. Kato, Y. Shimada, *et al.*, "A micro scanner with low power consumption using double coil layers on a permalloy film," in *Proc. IEEE-LEOS Conf. Opt. MEMS*, Aug. 2004, pp. 192–193.

[87] S. Hsu, T. Klose, C. Drabe, and H. Schenk, "Fabrication and characterization of a dynamically flat high resolution micro-scanner," *J. Opt. A, Pure Appl. Opt.*, vol. 10, no. 4, pp. 044005-1–044005-6, 2008.

[88] J. H. Park, J. Akedo, and H. Sato, "High-speed metal-based optical microscanners using stainless-steel substrate and piezoelectric thick films prepared by aerosol deposition method," *Sens. Actuators A, Phys.*, vol. 135, no. 1, pp. 86–91, Mar. 2007.

[89] T. Iseki, M. Okumura, and T. Sugawara, "High-speed and wide-angle deflection optical MEMS scanner using piezoelectric actuation," *Electr. Electron. Eng.*, vol. 5, no. 3, pp. 361–368, May 2010.

[90] T. Iseki, M. Okumura, and T. Sugawara, "Shrinking design of a MEMS optical scanner having four torsion beams and arms," *Sens. Actuators A, Phys.*, vol. 164, no. 2, pp. 95–106, Dec. 2010.

[91] S. Matsushita, I. Kanno, K. Adachi, R. Yokokawa, and H. Kotera, "Metal-based piezoelectric microelectromechanical systems scanner composed of Pb(Zr, Ti)O_3 thin film on titanium substrate," *Microsyst. Technol.*, vol. 18, no. 3, pp. 610–615, Jun. 2012.

[92] F. Filhol, E. Defay, C. Divoux, C. Zinck, and M. T. Delaye, "Resonant micro-mirror excited by a thin-film piezoelectric actuator for fast optical beam scanning," *Sens. Actuators A, Phys.*, vol. 123, pp. 483–489, Sep. 2005.

[93] C. D. Chen, Y. J. Wang, and P. Chang, "A novel two-axis MEMS scanning mirror with a PZT actuator for laser scanning projection," *Opt. Exp.*, vol. 20, no. 24, pp. 27003–27017, Nov. 2012.

[94] D. Jung, T. Sandner, D. Kallweit, H. Schenk, and F. I. Dresden, "Vertical comb drive microscanners for beam steering, linear scanning, and laser projection applications," *Proc. SPIE*, vol. 8252, pp. 82520U-1–82520U-10, Feb. 2012.

[95] S. Gu-Stoppel, J. Janes, D. Kaden, H. Quenzer, U. Hofmann, and W. Benecke, "Piezoelectric resonant micromirror with high frequency and large deflection applying mechanical leverage amplification," *Proc. SPIE*, vol. 8612, pp. 86120I-1–86120I-8, Mar. 2013.

[96] J. G. Smits, K. Fujimoto, and V. F. Kleptsyn, "Microelectromechanical flexure PZT actuated optical scanner: Static and resonance behavior," *J. Micromech. Microeng.*, vol. 15, pp. 1285–1293, May 2005.

[97] V. Milanovic, G. A. Matus, and D. T. McCormick, "Gimbal-less monolithic silicon actuators for tip-tilt-piston micromirror applications," *IEEE J. Sel. Topics Quantum Electron.*, vol. 10, no. 3, pp. 462–471, May 2004.

[98] J. Kim and L. Lin, "Electrostatic scanning micromirrors using localized plastic deformation of silicon," *J. Micromech. Microeng.*, vol. 15, no. 9, pp. 1777–1785, Jul. 2005.

[99] H. Miyajima, N. Asaoka, M. Arima, Y. Minamoto, K. Murakami, K. Tokuda, *et al.*, "A durable, shock-resistant electromagnetic optical scanner with polyimide-based hinges," *J. Microelectromech. Syst.*, vol. 10, no. 3, pp. 418–424, Sep. 2001.

[100] G. Reyne, "Electromagnetic actuation for MOEMS, examples, advantages and drawbacks of MAGMAS," *J. Magn. Magn. Mater.*, vol. 242, pp. 1119–1125, Apr. 2002.

[101] Y. Gokdel, B. Sarioglu, S. Mutlu, and A. Yalcinkaya, "Design and fabrication of two-axis micromachined steel scanners," *J. Micromech. Microeng.*, vol. 19, no. 7, pp. 075001-1–075001-8, Jun. 2009.

[102] N. Weber, H. Zappe, and A. Seifert, "An all-nickel magnetostatic MEMS scanner," *J. Micromech Microeng.*, vol. 22, no. 12, pp. 125008-1–125008-7, Oct. 2012.

[103] H. Y. Huang, T. L. Tang, W. L. Sung, H. Y. Lin, and W. Fang, "A magnetostatic 2-axis MEMS scanner with I-section rib-reinforcement and slender permanent magnet patterns," in *Proc. 16th Int. Solid-State Sens., Actuators, Microsyst. Conf.*, Beijing, China, 2011, pp. 2366–2369.

[104] N. Weber, D. Hertkorn, H. Zappe, and A. Seifert, "Polymer/silicon hard magnetic micromirrors," *J. Micromech. Syst.*, vol. 21, no. 5, pp. 1098–1106, Oct. 2012.

[105] U. Baran, D. Brown, S. Holmstrom, D. Balma, W. Davis, A. Mazzalai, *et al.*, "High frequency torsional MEMS scanner for displays," in *Proc. 25th IEEE Int. Conf. MEMS*, Paris, France, Jan./Feb. 2012, pp. 636–639.

[106] Y. Yasuda, M. Akamatsu, M. Tani, T. Iijima, and H. Toshiyoshi, "Piezoelectric 2D-optical micro scanners with PZT thick films," *Integr. Ferroelectr.*, vol. 80, no. 1, pp. 341–353, Jan. 2006.

[107] H. Urey and R. Sprague, "Biaxial MEMS raster scanner with linear ramp drive," in *Proc. IEEE/LEOS Int. Conf. Opt. MEMS*, Waikoloa, HI, USA, 2003, pp. 161–162.

[108] S. T. Hsu, T. Klose, C. Drabe, and H. Schenk, "Two dimensional microscanners with large horizontal-vertical scanning frequency ratio for high-resolution laser projectors," *Proc. SPIE*, vol. 6887, pp. 688703-1–688703-13, Feb. 2008.

[109] M. K. Brown and G. Mansouri, "Nonlinear dynamics and control of a dual-capacitively driven torsional MEMS scanning mirror," *Proc. SPIE*, vol. 4985, pp. 63–71, Jan. 2003.

[110] M. Scholles, A. Braüer, K. Frommhagen, C. Gerwig, B. Höfer, H. Lakner, *et al.*, "Design of miniaturized optoelectronic systems using resonant microscanning mirrors for projection of full-color images," *Proc. SPIE*, vol. 6288, pp. 628807-1–628807-12, Aug. 2006.

[111] M. Brown, M. Freeman, C. Zobkiw, and J. Lewis, "50.3: Image Quality Considerations in Bi-sinusoidally scanned retinal scanning display systems," *SID Symp. Dig. Tech. Papers*, vol. 33, no. 1, pp. 1320–1323, 2002.

[112] V. Milanović, "Multilevel-beam SOI-MEMS for optical applications," in *Proc. 9th IEEE Int. Conf. Electron., Circuits, Syst.*, Dubrovnik, Croatia, Sep. 2002, pp. 281–285.

[113] E. T. Carlen, K. H. Heng, S. Bakshi, A. Pareek, and C. H. Mastrangelo, "High-aspect ratio vertical comb-drive actuator with small self-aligned finger gaps," *J. Microelectromech. Syst.*, vol. 14, no. 5, pp. 1144–1155, Oct. 2005.

[114] W. Makishi, Y. Kawai, and M. Esashi, "Magnetic torque driving 2D micro scanner with a non-resonant large scan angle," in *Proc. Int. Solid-State Sens., Actuators, Microsyst. Conf.*, Jun. 2009, pp. 904–907.

[115] I. W. Jung, U. Krishnamoorthy, and O. Solgaard, "High fill-factor two-axis gimbaled tip-tilt-piston micromirror array actuated by self-aligned vertical electrostatic combdrives," *J. Microelectromech. Syst.*, vol. 15, no. 3, pp. 563–571, Jun. 2006.

[116] U. Krishnamoorthy, D. Lee, and O. Solgaard, "Self-aligned vertical electrostatic combdrives for micromirror actuation," *J. Microelectromech. Syst.*, vol. 12, no. 4, pp. 458–464, Aug. 2003.

[117] W. Piyawattanametha, P. R. Patterson, D. Hah, H. Toshiyoshi, and M. C. Wu, "Surface-and bulk-micromachined two-dimensional scanner driven by angular vertical comb actuators," *J. Microelectromech. Syst.*, vol. 14, no. 6, pp. 1329–1338, Dec. 2005.

[118] D. Hah, P. R. Patterson, H. D. Nguyen, H. Toshiyoshi, and M. C. Wu, "Theory and experiments of angular vertical comb-drive actuators for scanning micromirrors," *IEEE J. Sel. Topics Quantum Electron.*, vol. 10, no. 3, pp. 505–513, May 2004.

[119] J. Kim, H. Choo, L. Lin, and R. S. Muller, "Microfabricated torsional actuators using self-aligned plastic deformation of silicon," *J. Microelectromech. Syst.*, vol. 15, pp. 553–562, Jun. 2006.

[120] Y. Du, G. Zhou, K. L. Cheo, Q. Zhang, H. Feng, and F. S. Chau, "A 2-DOF circular-resonator-driven in-plane vibratory grating laser scanner," *J. Microelectromech. Syst.*, vol. 18, no. 4, pp. 892–904, Aug. 2009.

[121] W. O. Davis, O. M. O'reilly, and A. P. Pisano, "On the nonlinear dynamics of tether suspensions for MEMS," *J. Vibrat. Acoust.*, vol. 126, pp. 326–331, Jul. 2004.

[122] H. M. Jeong, Y. H. Park, Y. C. Cho, J. S. Hwang, S. M. Chang, S. J. Kang, *et al.*, "Slow scanning electromagnetic scanner for laser display," *J. Micro. Nanolith.*, vol. 7, no. 4, p. 043003, Dec. 2008.

[123] M. Tani, M. Akamatsu, Y. Yasuda, and H. Toshiyoshi, "A two-axis piezoelectric tilting micromirror with a newly developed PZT-meandering actuator," in *Proc. IEEE 20th Int. Conf. MEMS*, Kobe, Japan, Jan. 2007, pp. 699–702.

[124] T. Kobayashi, R. Maeda, and T. Itoh, "Low speed piezoelectric optical microscanner actuated by piezoelectric microcantilevers using $LaNiO_3$ buffered Pb(Zr, Ti)O_3 thin film," *Smart Mater. Struct.*, vol. 18, no. 6, pp. 065008-1–065008-6, 2009.

[125] N. Asada, H. Matsuki, K. Minami, and M. Esashi, "Silicon micromachined two-dimensional galvano optical scanner," *IEEE Trans. Magn.*, vol. 30, no. 6, pp. 4647–4649, Nov. 1994.

[126] J. Tsai, T. Hsieh, S. Chiou, D. Hah, and M. C. Wu, "Experimental characterization of two-axis MEMS scanners with hidden radial vertical combdrive actuators and cross-bar spring structures," *J. Micromech. Microeng.*, vol. 19, no. 4, pp. 045002-1–045002-12, Mar. 2009.

[127] H. Schenk, P. Durr, T. Haase, D. Kunze, U. Sobe, H. Lakner, *et al.*, "Large deflection micromechanical scanning mirrors for linear scans and pattern generation," *IEEE J. Sel. Topics Quantum Electron.*, vol. 6, no. 5, pp. 715–722, Sep./Oct. 2000.

[128] V. Milanovic, K. Castelino, and D. T. McCormick, "Highly adaptable MEMS-based display with wide projection angle," in *Proc. IEEE 20th Int. Conf. MEMS*, Kobe, Japan, Jan. 2007, pp. 143–146.

[129] W. L. Sung, T. L. Tang, F. Y. Lee, C. C. Tu, C. H. Huang, R. Chen, *et al.*, "Lorentz force torsional actuator with embedded nickel structures," in *Proc. IEEE Sensors*, Taiwan, Oct. 2012, pp. 1–4.

[130] J. Tsaur, L. Zhang, R. Maeda, and S. Matsumoto, "2D micro scanner actuated by sol-gel derived double layered PZT," in *Proc. 15th IEEE Int. Conf. MEMS*, Las Vegas, NV, USA, Jan. 2002, pp. 548–551.

[131] S. Gu-Stoppel, J. Janes, H. J. Quenzer, U. Hofmann, D. Kaden, B. Wagner, *et al.*, "Design, fabrication and characterization of low-voltage piezoelectric two-axis gimbal-less microscanners," in *Proc. 17th Int. Conf. Solid-State Sens., Actuators, Microsyst., Transducers Eurosensors*, Barcelona, Spain, 2013, pp. 2489–2492.

[132] K. Aksit, O. Eldes, S. Viswanathan, M. O. Freeman, and H. Urey, "Portable 3D laser projector using mixed polarization technique," *J. Display Technol.*, vol. 8, no. 10, pp. 582–589, 2012.

[133] M. K. Hedili, M. O. Freeman, and H. Urey, "Transmission characteristics of a bidirectional transparent screen based on reflective microlenses," *Opt. Exp.*, vol. 21, no. 21, pp. 24636–24646, Oct. 2013.

[134] H. Xie, G. K. Fedder, and Y. Pan, "MEMS-based endoscopic optical coherence tomography," *Proc. SPIE*, vol. 5721, pp. 81–92, Feb. 2005.

[135] H. Miyajima, K. Murakami, and M. Katashiro, "MEMS optical scanners for microscopes," *IEEE J. Sel. Topics Quantum Electron.*, vol. 10, no. 3, pp. 514–527, May 2004.

Sven T. S. Holmström received the M.Sc. degree in engineering biology from Linköping University, Linköping, Sweden, in 2005.

Since 2005, he has been a Research Engineer with the Optical Microsystems Laboratory, Department of Electrical and Electronics Engineering, Koç University, Istanbul, Turkey. He spent about one year as a Visiting Researcher at the École Polytechnique Fédérale de Lausanne, Lausanne, Switzerland, and four months at Chalmers University of Technology, Gothenburg, Sweden. He is the coauthor of 10 journal articles and 15 conference proceedings papers. He is the holder of a pending patent. His research interests include microfabrication and micro-optoelectromechanical systems.

Utku Baran received the B.Sc. and M.Sc. degrees both in electrical engineering from Koç University, Istanbul, Turkey, in 2010 and 2012, respectively. He is currently a Ph.D. candidate for the Department of Electrical Engineering, and a technology entrepreneurship certificate (TEC) student at the Foster School of Business at the University of Washington, Seattle, WA, USA.

He worked as an intern at Microvision Inc., Seattle, WA, USA; University of Tokyo, Tokyo, Japan; and North Carolina State University, Raleigh, NC, USA. He also spent four months at École Polytechnique Fédérale de Lausanne, Lausanne, Switzerland, as a visiting researcher. He is the author of five international journal articles, four peer-reviewed conference papers, and the co-inventor of two pending US patents. His interests include research and development of commercial devices using MEMS and/or medical imaging techniques, and technology commercialization.

Hakan Urey (M'92–SM'09) received the B.S. degree in electrical engineering from Middle East Technical University, Ankara, Turkey, in 1992, and the M.S. and Ph.D. degrees in electrical engineering from the Georgia Institute of Technology, Atlanta, GA, USA, in 1996 and 1997, respectively.

After completing the Ph.D. degree, he joined Microvision, Inc., Seattle, WA, USA, as a Research Engineer, and he played a key role in the development of scanning display technologies. He was the Principal System Engineer when he left Microvision, Inc. in 2001 to join the College of Engineering, Koç University, Istanbul-Turkey, where he established the Optical Microsystems Laboratory. He is currently a Professor of electrical engineering at Koç University. He has published more than 50 journal articles and more than 100 conference papers, six edited books, and four book chapters, and he has about 30 issued and pending patents, which have been licensed to industry for commercialization. His research interests are in microelectromechanical systems, micro-optics, microoptoelectromechanical systems design, and laser-based 2-D/3-D display and imaging systems.

Dr. Urey is a member of SPIE, OSA, the IEEE Photonics Society, and the Vice-President of the Turkey Chapter of the IEEE Photonics Society. He was the recipient of the Werner von Siemens Faculty Excellence Award from Koç University in 2006, Distinguished Young Scientist Award from the Turkish Academy of Sciences in 2007, Encouragement Award from The Scientific and Technological Research Council of Turkey (TÜBİTAK) in 2009, Outstanding Faculty of the Year Award from Koç University in 2013, and European Research Council-Advanced Investigator Grant in 2013.